Transformerless Current Source Converter-Based Battery Energy Storage Systems

by

Mohammadjavad Hassani

A thesis

presented to Lakehead University

in fulfillment of the

thesis requirement for the degree of

Doctor of Philosophy

Lakehead University, Thunder Bay, Ontario, Canada, 2025

Abstract

Conventional battery energy storage systems (BESSs) connected to medium-voltage ac grids, whether integrated with renewable energy sources (RESs) or used in battery charging applications, face several challenges, including the need for bulky low-frequency transformers (LFTs) to connect to the medium-voltage ac (MVAC) grid and high current stress. These issues arise because voltage source converter-based approaches typically operate at low battery string voltages due to constraints on the series connection of them. While multilevel topologies with independent batteries, such as cascaded H-bridge and modular multilevel converters, raise voltage by stacking series-connected modules, they introduce substantial complexity because continuous energy and state of charge (SoC) balancing are required through control or added hardware. To ensure reliable and stable operation, systems often use active balancing, coordinated control, and additional balancing circuits, and often include spare modules or module overdesign to enable bypass of faulty units. These measures increase hardware count, cost, and control burden, and can still be insufficient under multiple faults or severe SoC mismatch. Moreover, the proposed LFT-less solutions for charging batteries in battery swapping stations often rely on offline balancing methods during low-demand periods, leading to unnecessary charge-discharge cycles and accelerated degradation.

This work presents current source converter-based solutions for MVAC-connected applications that address these limitations without requiring LFTs, balancing controllers, or offline operation. First, a current source inverter-based BESS is proposed for the grid integration of RESs. The LFT requirement is removed, using a string of modular low-voltage battery packs to increase the voltage of the dc-link. By using the variable dc link, the system operates without SoC balancing requirements and tolerates pack bypass under faults or depletion without requiring additional

modules. Second, a current source rectifier-based battery charging system is proposed for a battery swapping station, addressing key challenges of the application. Third, a current source converter-based BESS is presented to address bidirectional power flow and energy arbitrage with the grid. The systems provide regulated currents and offer inherent short-circuit protection while interfacing with the MVAC grid. The proposed system's operating principles, control strategies, and design considerations are discussed, and their effectiveness for the next generation of grid-connected battery energy storage applications is demonstrated through theoretical analysis, simulation studies, and experimental validation.

To my family.

Acknowledgements

"Whoever enters the Way without a guide will take a hundred years to travel a two-day journey."

— Rumi

With deep appreciation for those who have significantly contributed to my academic journey, I wish to extend my sincere gratitude.

First and foremost, I would like to thank my supervisor, Dr. Qiang Wei, for his invaluable supervision, guidance, and encouragement throughout the course of my doctoral studies. His expertise, insightful feedback, and patient mentorship have been instrumental in shaping my research and helping me grow as a scholar. Conducting this work under his supervision has truly been an honor.

I am grateful to my colleagues and friends, whose encouragement, constructive discussions, and support have enriched this research and made the journey more rewarding.

Most importantly, I owe my heartfelt gratitude to my beloved parents and sisters for their unwavering love, prayers, and encouragement. Their belief in me has been a constant source of strength, and their happiness has remained the greatest motivation in my life. Words cannot fully express how grateful I am for their support throughout this long and challenging journey.

Contents

List of Tables

List of Figures

List of Abbreviations

2LVSI	Two-level voltage source inverter
ANPC	Active neutral point clamp
BESS	Battery energy storage system
BSS	Battery swapping system
CC	Constant current
CCD	Constant current discharge
CHB	Cascaded H-bridge
CPD	Constant power discharge
CSC	Current source converter
CSI	Current source inverter
CSR	Current source rectifier
CV	Constant voltage
EV	Electric vehicle
LFT	Low-frequency transformer
MMC	Modular multilevel converter
MVAC	Medium-voltage ac
MVDC	Medium voltage dc
RES	Renewable energy source
SGCT	Symmetrical gate-commutated thyristor
SLB	Second-life battery

SoC	State-of-charge
SVM	Space vector modulation
VSI	Voltage source inverter
ZSV	Zero-sequence voltage

List of Symbols

L_{dc}	dc-link inductor
L_f	Filter inductor
C_f	Filter capacitor
B_i	Battery in module *i*
Q_i	Switch in module *i*
D_i	Bypass diode in module *i*
d_i	Gate signal in Module *i*
v_{dc}	String voltage
V_{dc}	Average string voltage
i_{dc}	dc-link current
I_{dc}	Average dc-link current
i_{DC1}	Current of the first battery
I_{dc}	Average dc-link current
$V_{gL\text{-}L}$	RMS value of the grid line-to-line voltage
V_{rms}	RMS value of the grid line-to-neutral voltage
i_{w1}	CSC fundamental output current
I_{w1}	RMS of CSC fundamental output current
θ_{w}	CSI fundamental output current angle
α	Phase displacement between the grid voltage and the CSI fundamental output current
i_{dc}^{*}	dc-link current reference

P_g^*	Grid output power reference
P_g	Grid output power
P_{dc}	output power of the dc-link
i^*_B	battery's current reference
i_B	battery's current
V_B	battery's voltage
I_{rated}	battery's rated current
V_{rated}	battery's rated voltage
V_m	module voltage
m_a	modulation index
pu	Per unit

Chapter 1: Introduction

This chapter begins by examining the conventional structure of high-power medium-voltage ac (MVAC) grid-tied battery energy storage systems (BESSs), followed by a review of existing literature and recent advancements in the field. It highlights key technical challenges observed across current systems, their causes, and overall impact. Various solutions proposed in prior studies are also discussed. Based on this foundation, the chapter concludes by defining the primary research objective that frames the scope of this thesis.

1.1 Application Domains of BESSs

BESSs have emerged as a critical component in modern power and energy infrastructures, supporting a wide range of applications beyond conventional storage. This section highlights three distinct yet complementary use cases: (i) integration of renewable energy sources (RESs) into the grid; (ii) battery charging systems for electric vehicle (EV) swapping stations; (iii) second-life deployment of retired EV batteries, which enables cost-effective and sustainable energy storage solutions. Each application is discussed in detail in the following subsections.

1.1.1 BESS for Grid Integration of RESs

The intermittent nature of RESs presents stability problems for the grid. Integrating BESS into the grid can mitigate these issues. BESSs are generally integrated with RES in two main configurations, as shown in Fig. 1-1, in which the integration of RESs, battery storage, and MVAC grid is illustrated. In the first type, the BESS interacts directly with the grid to perform bidirectional energy arbitrage, charging during periods of low electricity prices or surplus generation and discharging during peak demand. In the second type, the BESS is integrated alongside RES for

output firming, curtailment mitigation, and energy shifting, improving the system's overall stability. The second type of configuration allows excess energy generated during high production periods to be stored and later supplied during low generation intervals or high load conditions [1].

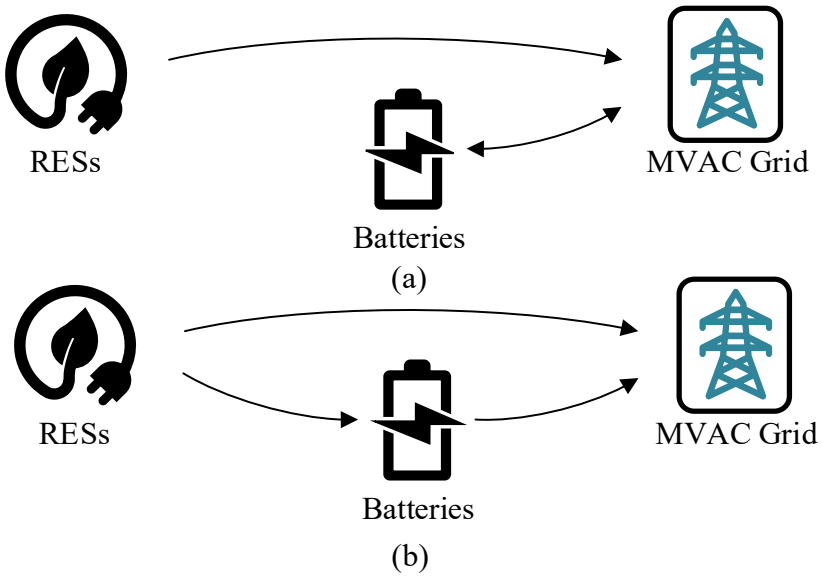

Fig. 1-1: Types of BESS integration in MVAC-connected RES-based systems. (a) RES with grid-interactive BESS and bidirectional energy arbitrage. (b) RES output firming and load shifting using BESS.

1.1.2 BESS Chargers for Battery Swapping Systems

Electric vehicles (EVs) offer zero emissions, lower lifetime costs, enhanced safety, and the ability to integrate into RESs, making them a promising alternative to traditional vehicles. In recent years, this has motivated a significant shift toward EV adoption [2]. Conventional plug-in EVs face constraints that can be resolved using the battery swapping system (BSS), though it has certain drawbacks.

A BSS can considerably reduce charging time, which remains a major holdup for EVs. Moreover, by separating the EV and the battery from each other, the car owners are relieved of

concerns related to battery degradation [3]. Optimized charge scheduling can help reduce costs by enabling off-peak charging and avoiding peak grid demand, thereby improving grid stability [4]. BSS can also service the power grid through frequency regulation [5], [6]. However, challenges include the high initial cost of stations, the need for battery standardization, and the requirement to maintain sufficient inventory during peak hours [7]. As a result, BSSs are more suitable for commercial fleet applications [8]. A BSS includes a station where depleted EV batteries are removed and replaced with fully charged units. The charged and discharged batteries are managed through a storage system and are then connected to a charger for recharging. The battery-swapping method for EV charging is presented in Fig. 1-2.

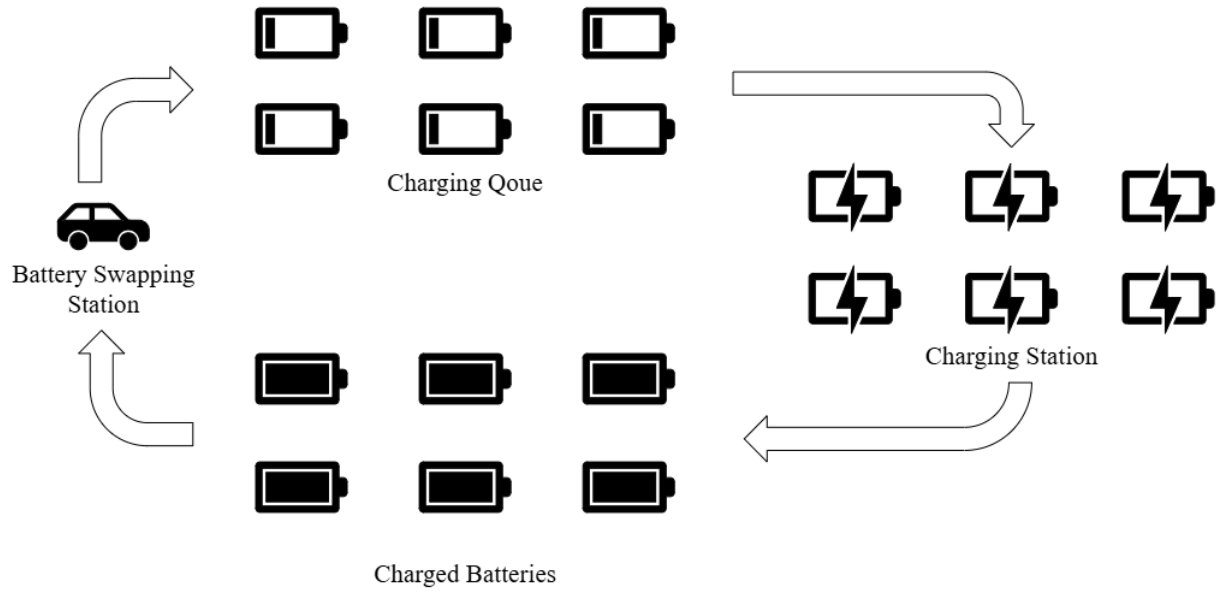

Fig. 1-2: Battery swapping system.

Battery swapping is active commercially. In China, two major providers have deployed extensive networks. NIO opened its first station in May 2018 and operated 190 stations by March 2021. Its second-generation station accommodates 13 battery packs and supports up to 312 swaps

per day. Aulton has commissioned more than 300 stations in cooperation with automakers and commercial EV operators, with deployments tailored to specific vehicle and battery types [7].

1.1.3 BESS Using Retired Lithium-ion EV Batteries

The increasing adoption of EVs has led to a corresponding surge in lithium-ion battery deployment. As these batteries reach the end of their automotive service life, typically when their capacities drop to around 70–80% of their nominal values, they can be repurposed for second-life battery energy storage systems, as they are insufficient for EV performance but still viable for less-demanding stationary applications [9]. Repurposing them for second-life applications has become a promising strategy to extend battery life, reduce environmental impact, and support growing energy storage demands.

Robust battery management systems tailored for heterogeneous cells are required to manage performance. Deploying second-life lithium-ion batteries (SLBs) is constrained by safety concerns and a higher probability of failure, which may result in system breakdowns or even catastrophic incidents. Partial charge-discharge strategies are adopted to mitigate these risks and reduce further degradation, wherein batteries operate within specifically restricted state-of-charge (SoC) and depth-of-discharge windows. This controlled cycling regime promotes safer operation and helps maintain long-term battery health [10].

1.2 Literature Review

1.2.1 Conventional Structures

Battery packs can be connected in parallel or in series to increase the power and energy capacity of the system. The capacity of each BESS string is limited by the battery pack with the lowest capacity; otherwise, battery overcharge or over-discharge may occur. The variation in battery pack

characteristics is caused by natural discrepancies in production, which increase as the batteries age [11], [12]. Block diagrams of two conventional systems are presented in Fig. 1-3

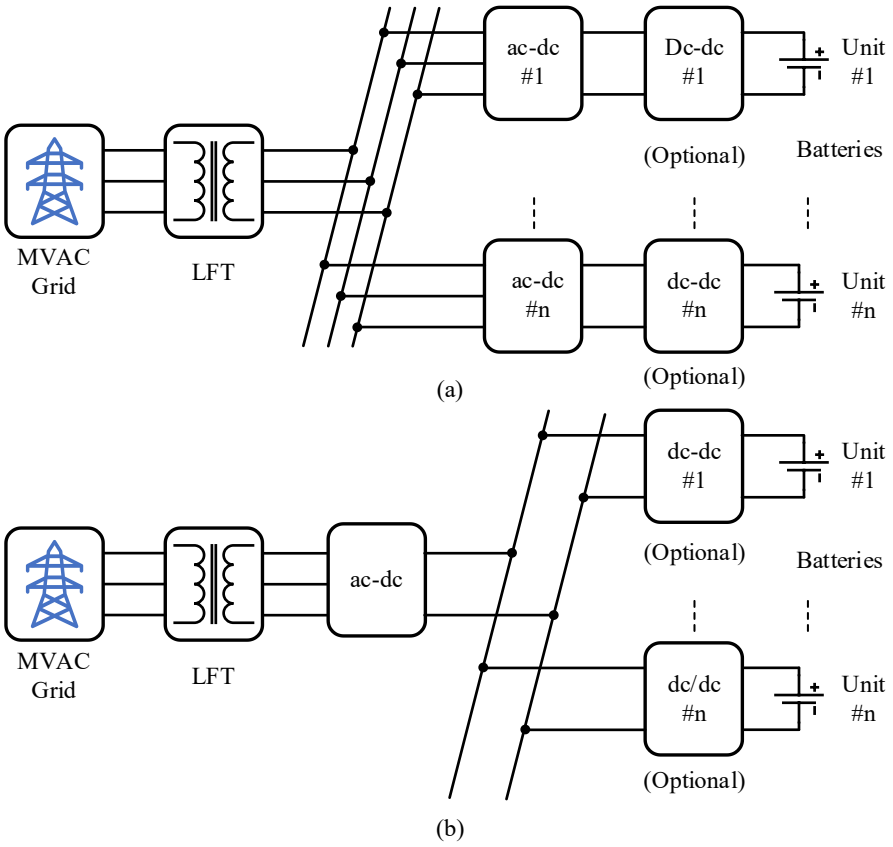

Fig. 1-3: Conventional BESSs. (a) A distributed ac-dc system with a common ac bus. (b) Centralized ac-dc system with a common dc-link.

Conventional utility-scale BESSs with a common dc-link typically employ a centralized power conversion architecture, where multiple battery strings are connected to a common dc-link and interfaced with the grid through two-level or three-level inverters, followed by low-frequency transformers (LFTs) for the MVAC connection. Common ac bus systems require multiple ac-dc converters [13]. The topology of the two-level voltage source inverters (2LVSI) and three-level active neutral point clamp (ANPC) BESS is presented in Fig. 1-4.

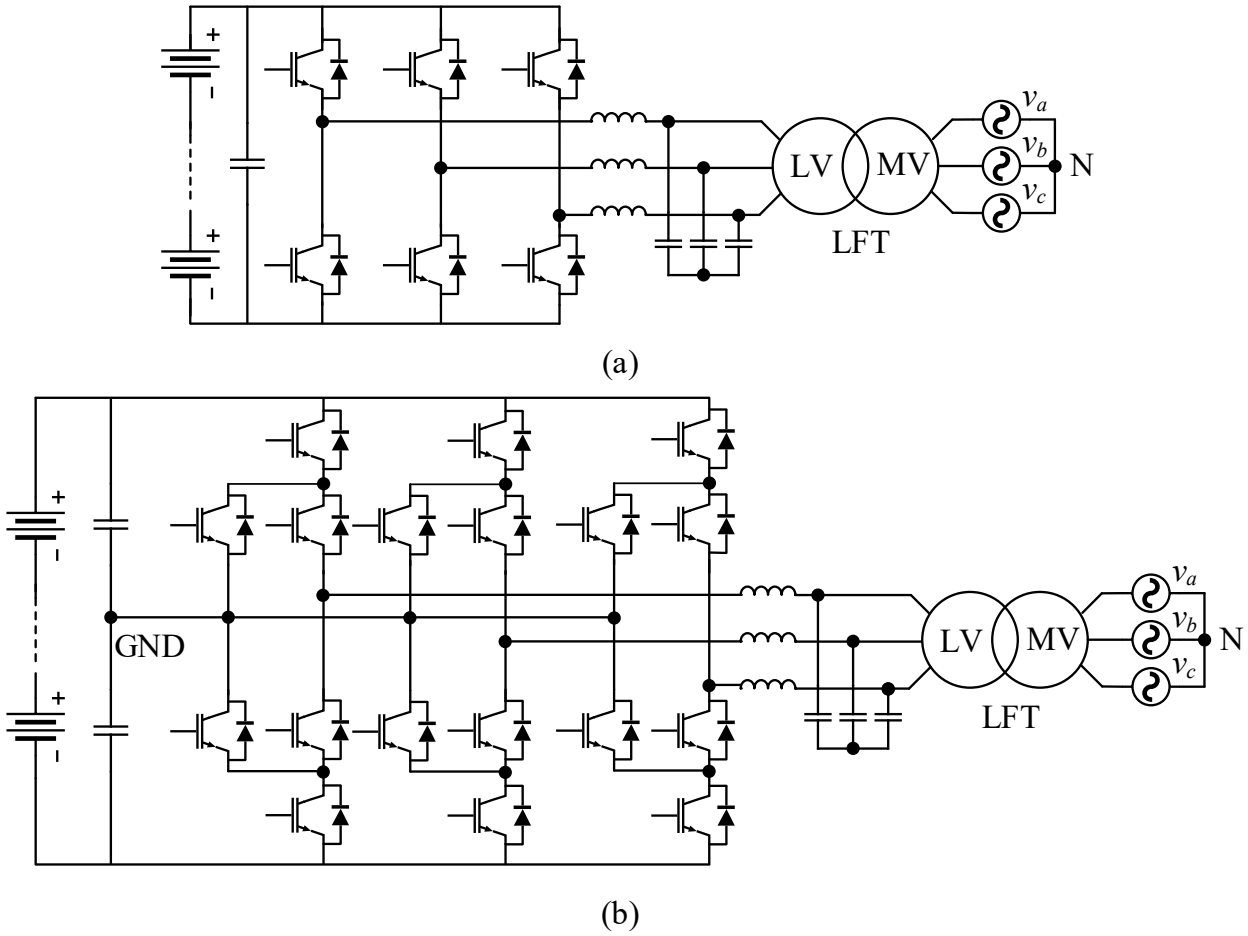

Fig. 1-4: Voltage source-based BESSs. (a) 2LVSI. (b) Three-level ANPC.

However, these systems suffer from high input current in high-power applications, and step-up dc-dc converters are required to eliminate the possibility of circulating current between parallel packs [14]. Additionally, centralized systems with parallel battery configurations offer limited flexibility in managing battery packs with heterogeneous characteristics [15], [16]. A dedicated connection of battery packs to the dc-link of the power conversion system through dc-dc converters enables independent control of charging and discharging power [14]. The LFTs are bulky, lossy, heavy, and require a large footprint [17] [18]. Also, the no-load operation of the transformer, which could be substantial in BESS, may increase the system's power loss [14]. Even though the ac bus system is more mature, systems with a common dc-link offer several advantages, including more

efficient integration of RESs, simplified control due to the absence of reactive power on the dc-link, and a single grid connection point. A similar classification can be extended to battery charging systems, where centralized and distributed configurations also exhibit comparable trade-offs. The same limitation of the LFT requirement for the MVAC connection also applies [19].

A few common industrial battery storage system configurations are illustrated here. One example is the PCS100 ESS, manufactured by ABB [20] , which consists of multiple parallel two-level voltage source inverters (VSIs). Its power rating ranges from 100 kVA to 4000 kVA, depending on the number of modules. The PCS100 is available in two dc voltage ranges: 250 V–820 V and 250 V–1120 V. The complete system design is shown in Fig. 1-5. An LFT is used to connect the system to the MVAC grid. The PCS100 does not incorporate a dc–dc stage; consequently, all batteries operate at a single operating point.

The LUNA2000-213KTL-H0 converter, manufactured by Huawei, is a dual-stage system integrating a boost converter with a three-level inverter [21]. This configuration raises the dc-side voltage to 800–1500 V and produces an ac-side output of 800 V. Each unit delivers up to 213 kW of power. For grid connection, Huawei offers step-up transformers such as the JUPITER-9000K-H0. This 9 MVA transformer supports up to 44 low-voltage inputs and has a total weight of less than 28 t. The complete system configuration is shown in Fig. 1-6. Huawei also supplies battery strings compatible with this system, an example of which is summarized in Table 1-1.

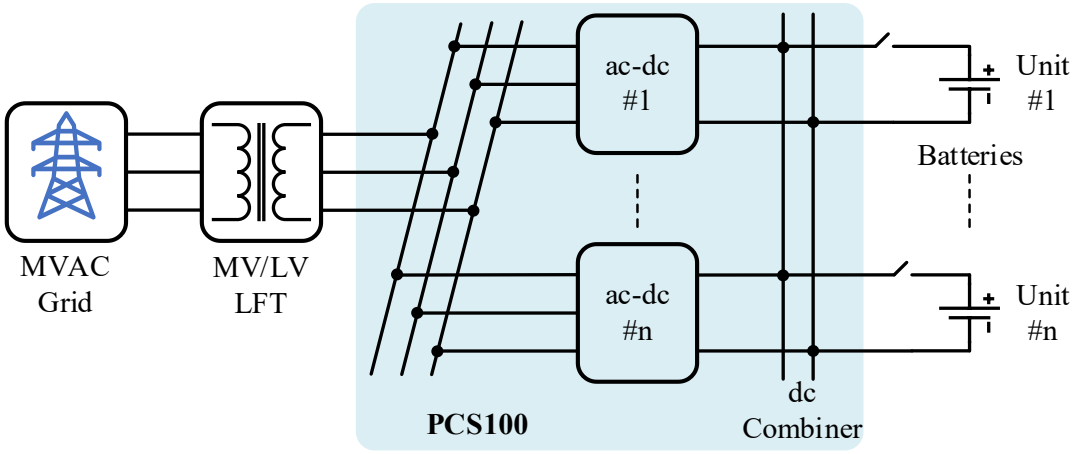

Fig. 1-5: Utility-scale battery energy storage system using PCS100 ESS.

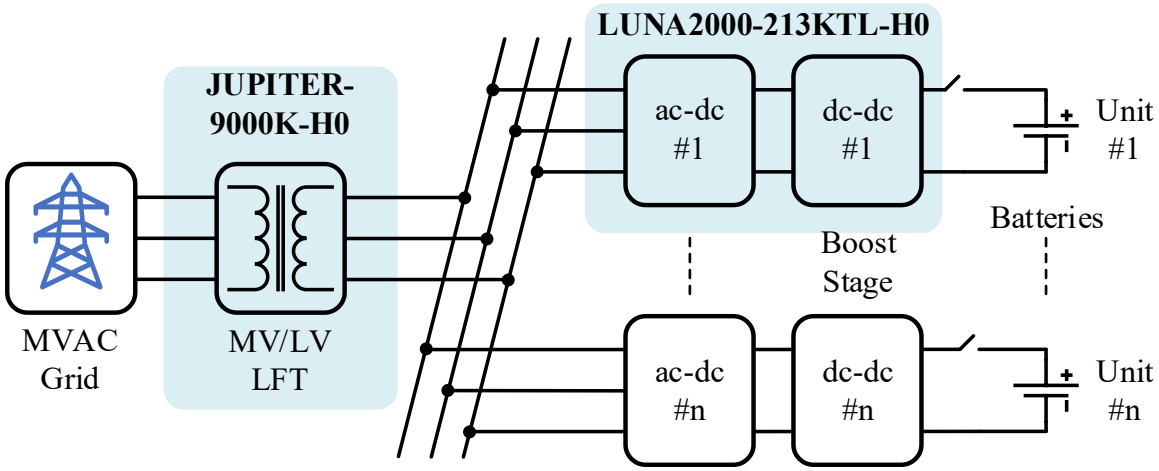

Fig. 1-6: Utility-scale battery energy storage system using LUNA2000-213KTL-H0 converter and JUPITER-9000K-H0 transformer.

1.2.2 Modular Multilevel-based Transformerless Converters

A cascaded H-bridge converter (CHB), as presented in Fig. 1-7(a) [22], [23], [24], [25] or a modular multilevel converter (MMC) [26] (Fig. 1-7(b)) can be used to increase the voltage levels and eliminate the need for an LFT in BESSs or hybrid RES + BESSs [27], [28], [29]. As shorter battery strings can be used, each cell's input and power output can be controlled separately.

High-voltage level ground insulation for the converters and battery packs would be required, as the battery strings are not grounded, which is provided by additional insulation measures between the cells, and the ground support brackets [14].

TABLE 1-1. Utility-scale battery string by Huawei

Battery string name	LUNA2000-2.0MWH-2H0
DC rated voltage	1200 V
DC maximum voltage	1500 V
Nominal energy capacity	2064 kWh (6 × 344 kW)
Rated power	2064 kW
Rated voltage of a battery rack	1075.2 V (907 – 1227 V)
Number of battery racks per ESS	6
Battery pack configuration	One battery rack is configured with 21 battery packs (126 packs in total)
Battery pack rated voltage	51.2 V

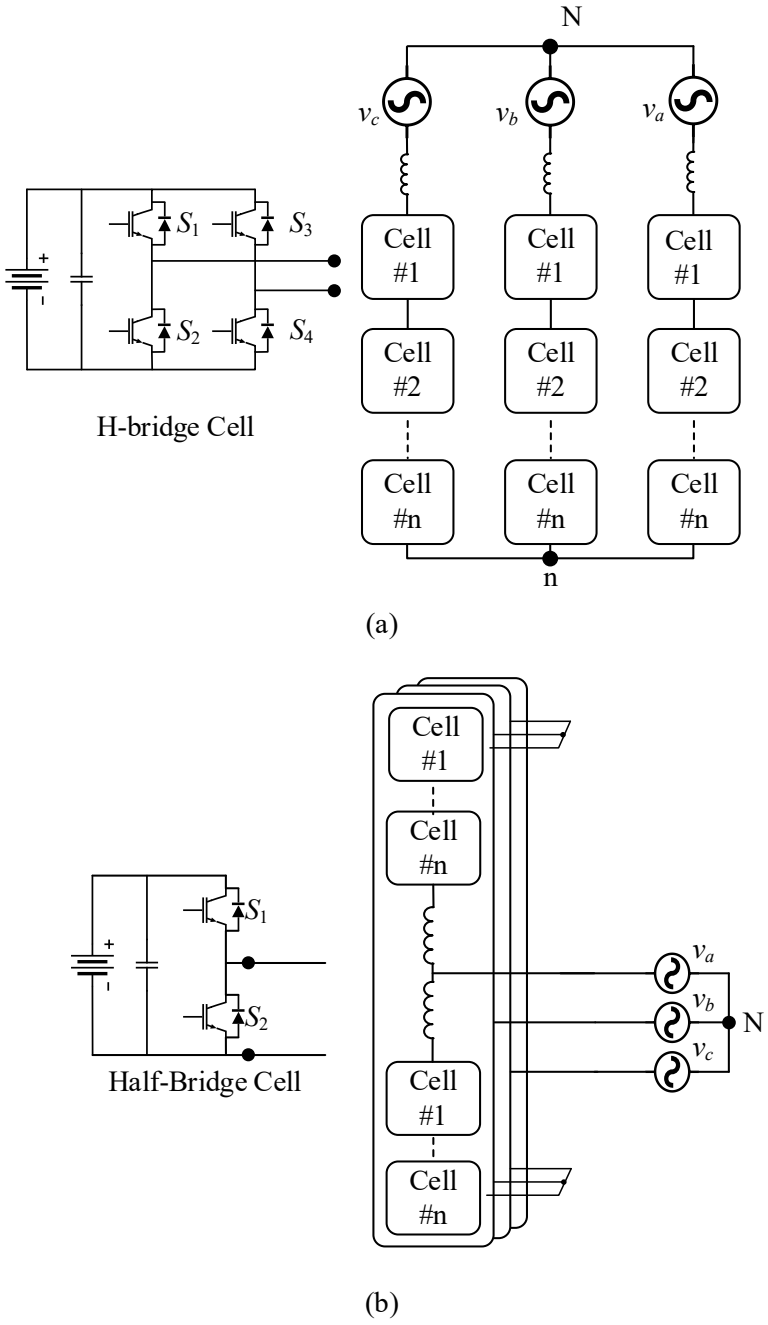

Fig. 1-7: Grid-tied BESS. (a) CHB. (b) MMC.

Even though the modular structures have advantages such as low switching frequency and low switch voltages, complex control of each module is required. Using constrained cycling methods to help preserve battery health when using second-life batteries (SLBs) can further aggravate this issue [30], [31], [32], [33]. Variations in allowable SoC ranges and capacities among system

battery modules can cause energy imbalances across converter arms and submodules. This complicates power sharing and may result in voltage and power mismatches, waveform distortion, reduced system capacity, and increased control complexity. To ensure reliable and stable operation while using SLBs, sophisticated active balancing schemes, coordinated control strategies, or additional balancing circuits are required [34], [35], [36], [37], [38], [39].

Another drawback of directly connecting the batteries to the half-bridge or H-bridge modules in CHB- and MMC-based BESSs is the presence of second-order harmonics in the battery current, leading to faster battery degradation [40], [41]. Besides, the fault tolerance capability of the inverter is essential because of the possibility of battery module failure. Bypassing faulty modules could lead to output voltage and current distortion or even system shutdown. As a result, extra redundant modules or module overdesign would be necessary for modular converters to bypass the faulty ones [42].

In modular BESSs, individual batteries may reach their end-of-life (EoL) at different times due to inherent differences in degradation rates, especially in SLB applications, where remaining useful life variation is inherently larger. Weaker modules experience higher stress, which accelerates their degradation and can potentially trigger premature EoL for the entire system [12]. Compared to parallel topologies, this limitation reflects a key shortcoming of CHB and MMC modular BESS architectures, where series-connected submodules could constrain system performance based on the weakest module. Since all submodules contribute to the output voltage, the failure or early EoL of a single battery module can compromise the operation of the entire string, often requiring costly bypass mechanisms and redundancy provisions. This may include redundant units and circuitry [43] or control schemes that, upon fault detection, bypass the affected converter cell and generate alternative switching states to restore voltage balance.

Recent studies have proposed various converter topologies and control strategies to address these issues. A modular boost multilevel buck converter integrated with a grid-tied inverter is presented in [44], where each dc-dc module contains one SLB, and the modules are connected in series to form a common dc-link. A control strategy is also implemented to regulate battery charging and discharging while balancing SoC across modules. To address the SoC imbalance within CHB architectures, [45] proposes a coordinated modulation strategy to equalize SoC at both the interphase and interbridge levels. This approach mitigates interphase imbalances using a zero-sequence voltage (ZSV) injection technique. At the same time, individual cell-level balancing is achieved by injecting small sinusoidal voltages into each H-bridge cell within a cluster. The sum of these injected voltages across all cells in a cluster is zero, ensuring that the phase voltage remains unaffected.

An alternative SoC balancing approach is presented in [46], where optimized modulation techniques are applied to CHB BESSs. The control algorithm dynamically selects among multiple switching configurations that synthesize the same output voltage level, enabling SoC-dependent modulation in which higher-SoC batteries are subjected to increased discharge duty. The authors in [47] present a model predictive control (MPC) scheme for star-connected CHB systems, embedding a coordinated battery cell selection mechanism into the MPC framework to adjust each battery's contribution based on its SoC dynamically. Similarly, in [24] a dual-stage MPC strategy is proposed for SoC balancing in a delta-connected CHB BESS. The first stage computes an optimal circulating current reference to reduce interphase SoC imbalance, while the second stage determines modulating signals for inter-bridge balancing. [48] presents a SoC balancing method tailored for MMC architectures. This approach injects controlled ac and dc circulating currents

into the converter. The dc component equalizes SoC across different converter legs, while the ac component balances SoC between each leg's upper and lower arms.

These balancing control systems encounter limitations under extreme SoC imbalance or battery fault conditions, primarily due to power transfer boundaries inherent in multilevel converter structures. References [49], [50] discuss the issue of constrained power distribution in modular BESSs and propose methods to ensure that submodule power references remain within converter-imposed disparity limits and safe operating regions. ZSV injection methods are commonly applied to improve system resiliency during faults, too. Among various ZSV techniques, the fundamental frequency ZSV injection is the most widely employed technique [25], [42]. Nevertheless, even these advanced balancing mechanisms do not ensure reliable operation under severe imbalance or fault scenarios.

In [51] a three-port converter that balances power between the upper and lower arms of the MMC is proposed. However, it does not resolve intra-arm mismatches, as power imbalances among modules within the same arm remain unaddressed. Next, in [52] a bidirectional three-port MMC-based converter is introduced, designed to maintain power balance across the converter. While effective in achieving global balancing, this approach involves a complex interface and control architecture, which can limit its practicality for large-scale applications.

1.2.3 VSI-based Transformerless Converters

The other solution for a transformerless MVAC connection is to use a string of battery packs, directly connected to the medium-voltage dc (MVDC) grid, connected to a two-level or three-level VSI. Series-connected switches can be used to increase the voltage level of the inverter. Due to the voltage-boosting nature of these rectifiers, the dc-link voltage of the system becomes substantially high. Various types of configurations, including direct series pack connection, pack

bypass method, centralized dc-dc converter, or modular dc-dc converter, could be used, as shown in Fig. 1-8 [14], [53].

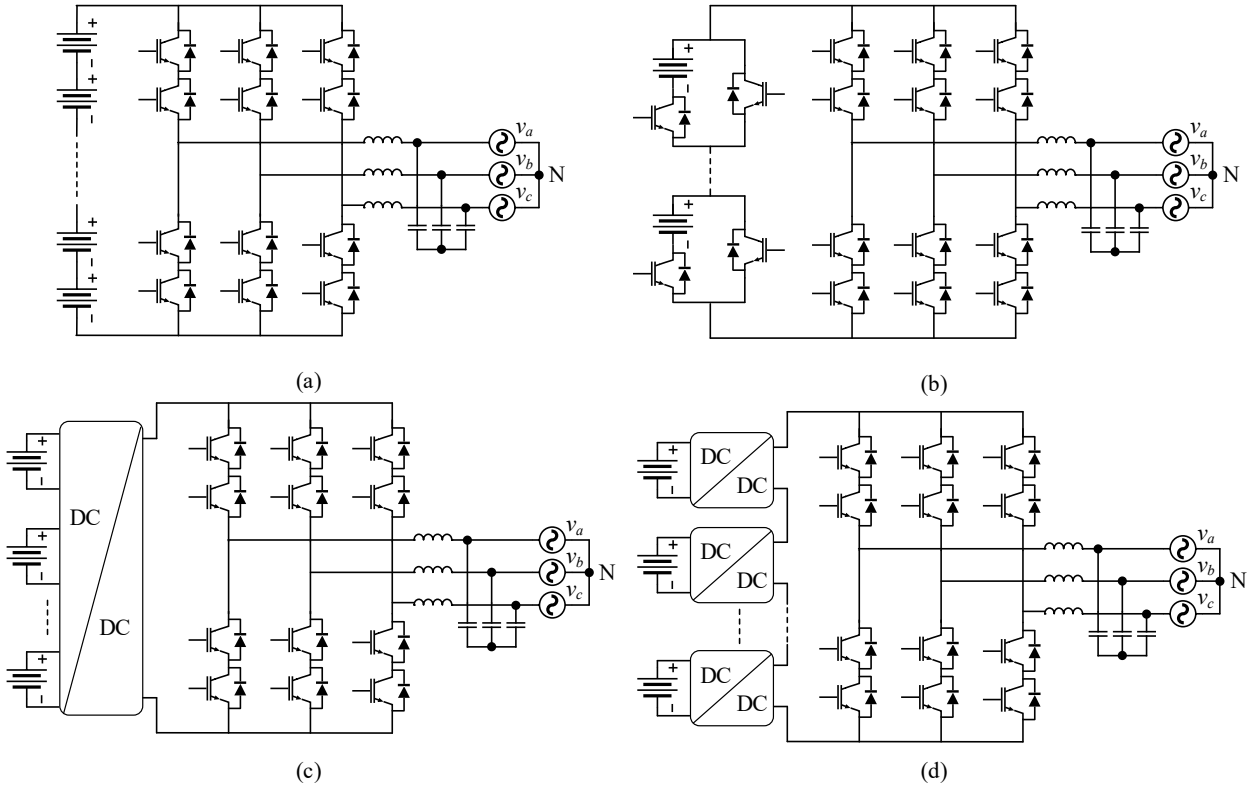

Fig. 1-8: Grid-tied BESS. (a) Direct series packs. (b) Pack bypass method. (c) Packs with a central dc-dc converter. (d) Packs with modular dc-dc converters.

VSIs with a series connection of packs (see Fig. 1-8(a)) have the advantage of simplicity, and they can be connected to the MVAC grid using a long string of battery packs. The battery string length and the inverter require considerable overdesign due to the inherent large variations in battery voltages. Also, in a large string of battery packs, the capacity of the string would be limited by the weakest pack. Furthermore, the failure of a pack or a cell will necessitate the elimination of the string by the battery management system, reducing reliability [54].

The pack bypass method proposed in [55] (see Fig. 1-8(b)) uses two IGBTs in parallel and in series of each battery pack to disconnect the cells in case of failure or pack depletion. Online

battery management could also be implemented to balance battery packs. However, in cases where several packs are disconnected, the voltage of the string would be reduced to below the minimum requirement of the inverter due to the variable voltage of the cell. This issue necessitates using an extra dc-dc stage (see Fig. 1-8(c)) to increase the voltage of the dc-link. Adding a central dc-dc converter would require a converter that supports high voltage and power stress.

Another method to incorporate separate battery packs instead of a long string is modular dc-dc converters (see Fig. 1-8(d)). The modular structure has the benefit of reduced voltage stress on the converters. However, in case of a large power mismatch between the modules or module failure, some modules may be bypassed. In that case, the dc-link voltage falls. The remaining modules must then raise the voltage to the inverter setpoint, which demands converter overdesign or additional backup modules and therefore increases cost [56].

To address the over-design issue in input-series BSS chargers, a charging system was proposed in [57], [58], as shown in Fig. 1-9. In this system, half-bridge modules operate at a constant duty cycle. Once batteries are fully charged, they are swapped with empty ones. However, charging is halted when the number of empty batteries falls below the required MVDC voltage threshold, indicating a period of low swapping demand. To solve this issue, a two-mode balancing control scheme is introduced. Specifically, the system switches to off-grid mode during such periods, enabling an internal energy transfer loop that charges low-SoC batteries using energy from high-SoC ones to equalize the SoCs and increase the number of swappable batteries. However, this internal circulation leads to unnecessary discharge cycles for the batteries, which reduces battery lifespan.

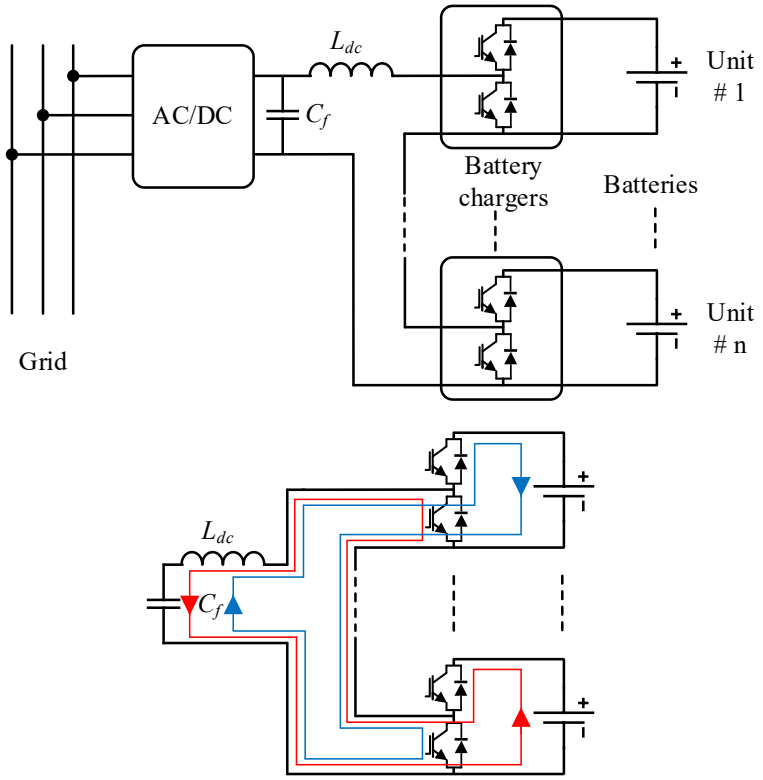

Fig. 1-9: Two-mode offline balancing charger for BSS systems.

Power-balancing strategies proposed for CHB and MMC topologies [42], [59], [60] primarily developed for renewable energy systems, battery storage systems, or fault-tolerant applications, remain limited and are ineffective for BSSs under low-demand conditions or when the number of available batteries is low. Offline SoC balancing can also be implemented in MMCs using circulating current, as shown in Fig. 1-10 [61]. In this case, however, the system is disconnected from the grid and operates in offline mode, where redundant charging and discharging of high-SoC batteries occur, which negatively affects battery lifespan.

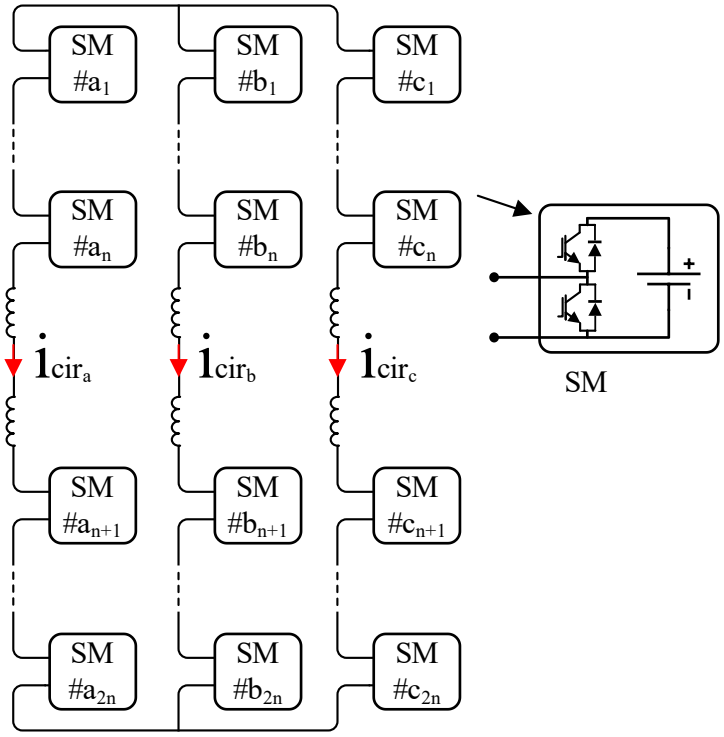

Fig. 1-10: Offline balancing the MMC system.

1.3 Technical Challenges and Research Objectives

High-power BESSs are increasingly deployed to support grid applications such as renewable energy integration and supporting emerging electrification needs. Conventional BESS architectures typically interface with the MVAC grid using LFTs. While this approach is well established, it introduces limitations in terms of increased system cost, size, and current stress. LFTs are bulky, heavy, and inefficient under light load conditions.

Transformerless topologies, such as MMC-based and CHB-based systems, provide an alternative by enabling direct connection to the MVAC grid. However, their integration with battery storage systems, especially those utilizing heterogeneity SLBs, presents several challenges. SLBs exhibit wide capacity variations, leading to SoC and power imbalance across modules. This

complicates power distribution among modules and can lead to voltage imbalance, power mismatch, waveform distortion, greater control complexity, reduced system utilization, or even system shutdown. To ensure reliable and stable operation, sophisticated active balancing schemes, coordinated control strategies, overdesigned components, additional balancing circuits, or redundant converter cells to bypass faulty or degraded modules are required to address reliability and voltage constraints. Proposed balancing schemes, such as circulating current control, coordinated modulation, and ZVS injection methods, partially mitigate inter-arm and inter-phase imbalance but remain inadequate under extreme mismatch or battery faults.

The objectives of this research are to:

- Develop a high-power MVAC-connected BESS architecture that eliminates the need for LFTs
- To eliminate the need for complex balancing control strategies and hardware by enabling reliable operation under SoC and capacity imbalance without active balancing circuits, coordinated modulation schemes, or redundancy provisions. including in applications where second-life lithium-ion battery modules are used.
- Investigate the performance of the proposed system under various grid-connected charging/discharging scenarios through simulation and experimental studies.
- Demonstrate the feasibility of the converter topologies and control methods in various use cases.

Building on the literature review and defined research objectives, this thesis introduces three novel low-frequency transformerless BESS architectures tailored for different applications, designed to eliminate module-level power imbalance. Fig. 1-11 presents a flowchart that summarizes the thesis structure and design progression. It begins with the identified gap and

objectives, followed by the three research contributions. The chart highlights the main targets of each chapter while indicating shared methods.

- The first contribution of this thesis is a current source inverter (CSI)-based BESS proposed for the grid integration of RESs. The system eliminates LFT and leverages the variable dc-link to operate without SoC balancing and is capable of bypassing depleted or faulty modules. The BESS operates with RESs to smooth output and shift energy, acting as a buffer between variable sources such as PV and wind and the MVAC grid.
- The second contribution is a current source rectifier (CSR)-based charger for battery swapping stations. This topology similarly removes the transformer and mitigates the SoC imbalance and the offline balancing challenges of conventional designs. It provides charging for non-uniform batteries with various charging profiles.
- Finally, a CSC-based modular BESS is presented to support second-life battery applications, bidirectional power flow, and energy arbitrage with the MVAC grid.

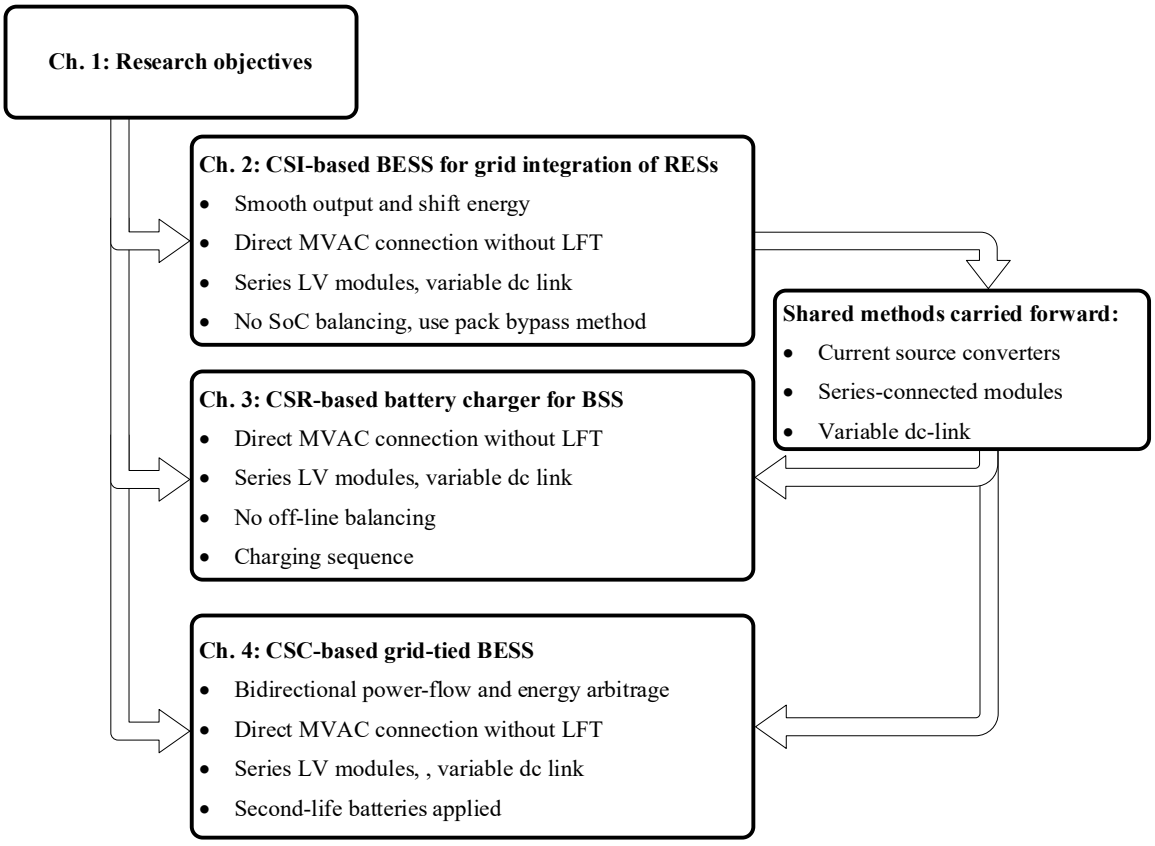

Fig. 1-11: thesis structure and design progression flowchart.

1.4 Chapter Summary

This chapter introduced the motivation and background for developing a new high-power BESS architecture suitable for direct MVAC grid connection. The discussion began with an overview of the conventional LFT-based structures and application domains of BESSs, followed by a review of transformerless modular converter topologies, such as CHB and MMC, and discussed their challenges related to SoC imbalance, fault tolerance, and converter-level power mismatch. Based on this analysis, the chapter concluded by formulating the research problem and outlining the main objectives of this thesis.

Chapter 2: A Current Source Inverter-Based BESS for Grid Integration of RESs

The previous chapter provided an overview of conventional high-power BESS architectures for MVAC grid integration, including LFT-based, LFT-less, and modular systems. It outlined key technical limitations such as high current stress, system cost, complex balancing requirements, and vulnerability to SoC imbalance.

This chapter presents a transformerless battery storage system for renewable energy integration utilizing a CSI and series-connected modular battery packs, which removes the requirement for an LFT and adeptly addresses the previously identified challenges. The topology is designed to accommodate the removal of failed or depleted battery packs without experiencing any adverse effects, and it eliminates the need for additional balancing control or circuits.

2.1 Principle of Operation

The configuration of the proposed system is presented in Fig. 2-1. The proposed system is based on the second type of integration shown in Fig. 1-1, where the BESS operates alongside RES to firm output and shift energy. In this configuration, batteries serve as an intermediate stage between the variable output of RESs, such as photovoltaic and wind systems, and the MVAC grid. The figure outlines the system configuration that enables the subsequent implementation of a modular CSI-based BESS, where energy from distributed sources is aggregated and delivered to the grid through a CSI. The proposed system consists of series-connected modules and a grid-tied CSI inverter. The CSI comprises a dc-link inductor (L_{dc}), six reverse-blocking switches, and filter inductors and filter capacitors (L_f, C_f). The CSI is a well-proven inverter commonly used in high-

power medium voltage applications, and it can be adapted for the proposed system. The CSI benefits from a simple structure, inherent short-circuit protection, and a grid-friendly waveform. CSI is well established for operation within the 2.3 to 6.6 kV range and typically handles power levels between 1 MW and 4 MW [62]. Commercial implementations further validate their practicality. For instance, Rockwell Automation Canada employs CSI-based drive systems that use series switch configurations—four switches per leg for 4.16 kV and six per leg for 6.6 kV grid connections. The reverse-blocking switches are implemented using symmetrical gate-commutated thyristors (SGCTs) rated at 6.5 kV. The current rating of the SGCTs varies depending on the drive specification, options include 400 A, 800 A, and 1500 A devices. This highlights the scalability and adaptability of CSI technology, making it a strong candidate for integration into the proposed system architecture.

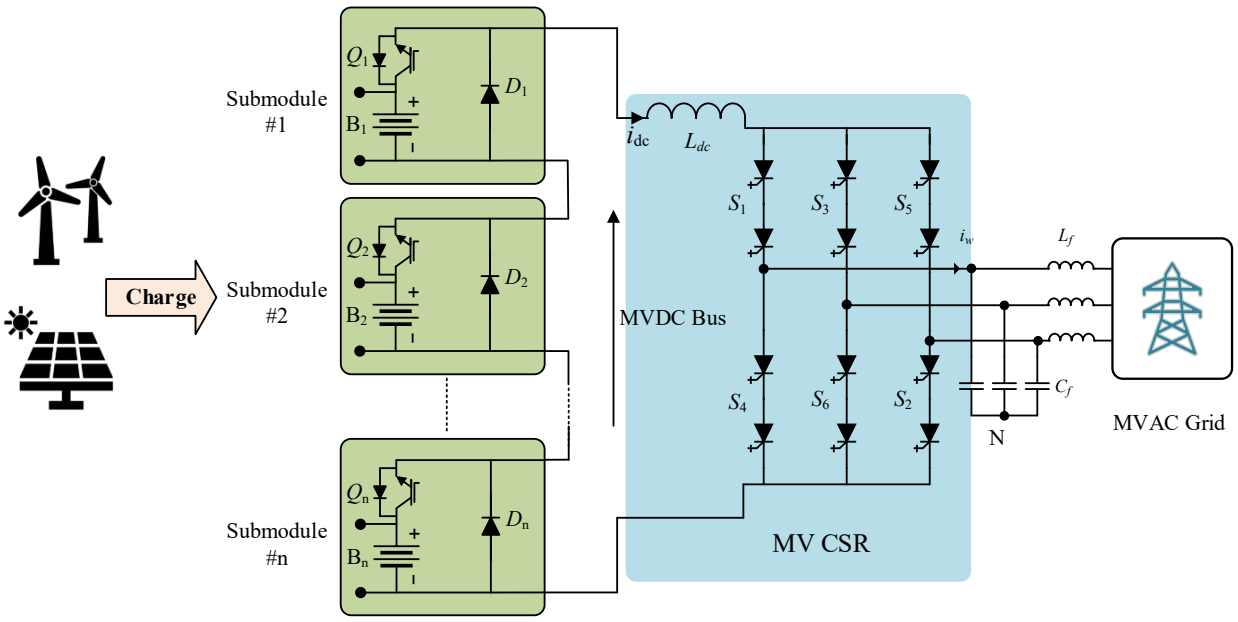

Fig. 2-1: Proposed CSI-based MVAC-tied BESS.

The module comprises a battery pack (B_i) with a series-connected switch (Q_i) and a bypass diode (D_i). In the proposed structure, battery packs serve as the intermediate stage for integrating

intermittent RESs such as photovoltaic and wind systems. Isolation stages are not required between the battery packs and the MVAC grid with the implementation of an insulation layer between modules and ground [14]. Series-connected modules produce a variable voltage medium voltage dc-link (MVDC).

By connecting several low-voltage modules in series and achieving an MVDC voltage, the requirement for an LFT is eliminated. In the proposed topology, each battery pack can either be included in the string or bypassed if it is empty or faulty. The proposed topology inherently avoids power and voltage imbalance issues, as it is not constrained by the performance of any single pack in the series string. This operation is enabled by a variable dc-link voltage of CSI, which allows the system to maintain continuous operation by bypassing depleted packs without the need for additional balancing mechanisms. The inverter can support the grid current even with lower string voltage owing to CSI's inherent boosting capability.

The operation modes of the battery module can be divided into two categories, as shown in Fig. 2-2. In mode (a), the module is active, the switch conducts, and the battery is connected, allowing it to be charged from RESs and to supply power to the grid. In mode (b), the battery is bypassed by the diode and isolated from the circuit. Once adequately charged, it can be reconnected to supply the grid.

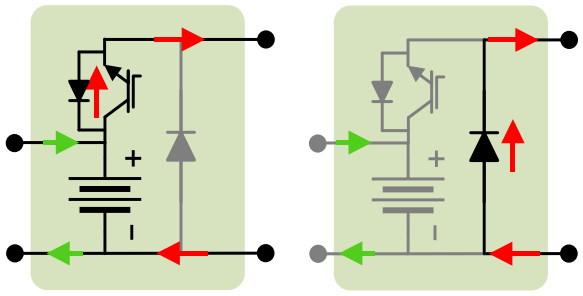

Fig. 2-2: Battery modules' modes of operation.

An example of the operation condition in the proposed converter is presented in Fig. 2-3, in which n battery modules are connected in series to the MVAC grid-tied CSI. Each battery pack module works in two modes. If a battery's state of charge (SoC) is below the threshold or the battery is at fault, the switch will be turned off, and the continuous current operation of the string will turn on the parallel diode. Otherwise, the switch will stay on, and the battery pack will remain in the string. The switch does not have a high-frequency switching operation, so the module does not have switching losses. In Fig. 2-3, the first module operates in bypass mode, and its battery (B_1) is disconnected, while the second and last modules are in active mode, and B_2 and B_n are discharging. All the active packs will have similar currents due to the constant current operation of the CSI dc-link. If the number of active modules decreases, the voltage of the string will decline.

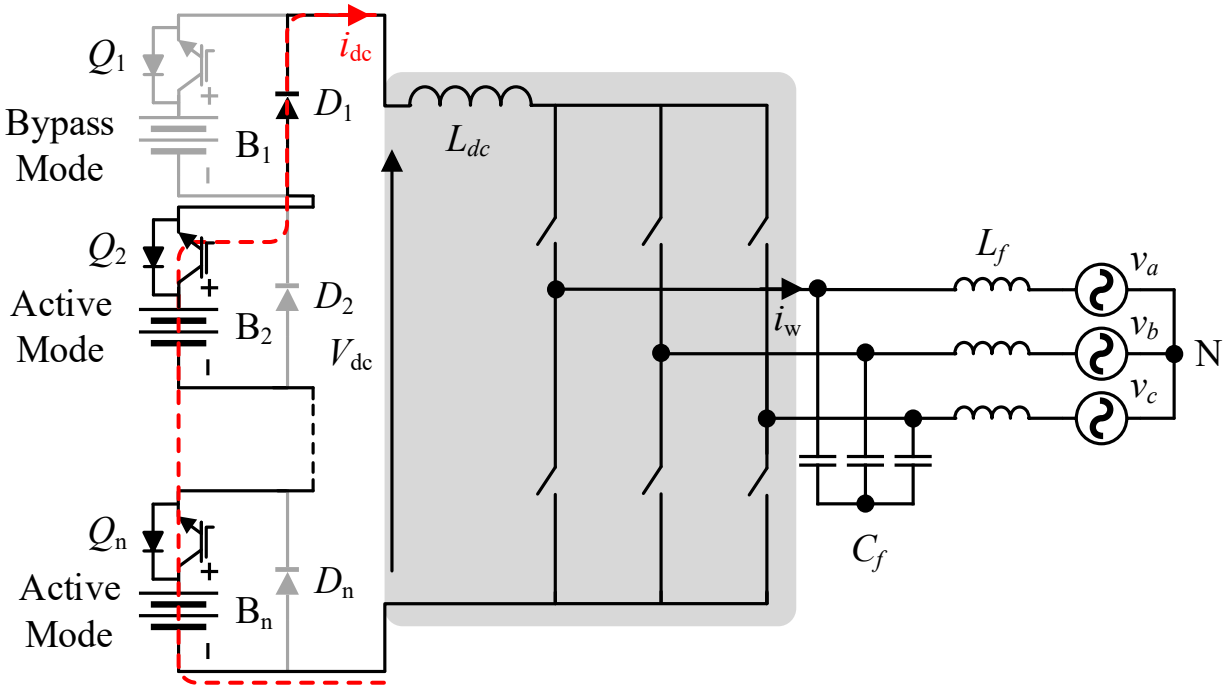

Fig. 2-3: Example of the system operation.

2.2 Design Considerations

A comparison between designing the battery string for the proposed CSI-based system and a VSI-based one is made to express the effectiveness of the operation. Considering V_{dc} as the average string or dc-link voltage, I_{dc} as the average dc-link current, V_{rms} as the RMS value of the grid line to neutral voltage, and α as the phase displacement between grid voltage, m_a as the modulation index of the CSI, i_{w1} as CSI's fundamental output current, and I_{w1} as the peak fundamental output current, the grid output power (P_g) can be expressed as:

$$P_g = 3V_{rms}I_{w1}\cos(\alpha) \tag{2-1}$$

The dc-link output power is equal to,

$$P_{dc} = V_{dc}I_{dc} \tag{2-2}$$

Neglecting the power losses, the grid and dc-link power outputs should be equal, thus,

$$V_{dc} = 3V_{rms}\frac{I_{w1}}{I_{dc}}\cos(\alpha) \tag{2-3}$$

The modulation index is equal to:

$$m_a = \frac{\sqrt{2}I_{w1}}{I_{dc}} \tag{2-4}$$

from which:

$$V_{dc} = (3/\sqrt{2})V_{rms}m_a\cos(\alpha) \tag{2-5}$$

Considering $m_a \leq 1$, the proposed system is operational as long as the voltage of the string satisfies:

$$V_{dc} \leq (3/\sqrt{2})V_{rms}\cos(\alpha) \tag{2-6}$$

Comparatively, two-level VSIs (2LVSIs) require a V_{dc} that is:

$$V_{dc} \geq (\sqrt{6})V_{rms} \tag{2-7}$$

For a practical comparison, several assumptions are made.

- The MVAC line-line voltage of the grid ($V_{gL\text{-}L}$) is 4160 V.
- The operating range of a Li-ion battery cell is between 3 V and 4.2 V. Each battery pack consists of 200 cells (600-840 V), consistent with the voltage range of 800 V batteries.

Based on these assumptions and equations (2-6) and (2-7), the proposed system can operate with up to six series-connected battery packs, while a VSI-based system requires at least ten. As a result, the proposed system can reduce the number of series-connected cells by at least sixty percent, assuming all battery packs are discharged simultaneously. In this way, the proposed system requires a shorter battery string and a lower dc-link voltage. However, in the case of unbalanced SoCs, some battery packs may deplete faster. Also, some battery packs may become faulty and have to be bypassed. In such cases, the VSI-based system requires additional redundant series-connected packs, increasing the string length to support the grid or risk system shutdown. However, the proposed system has no such drawback and can continue operation even to the last available module. Also, no complex active balancing strategies are required.

The switch and diode inside the modules only have to withstand the maximum voltage of the battery pack. As a result, a single 1200V IGBT and diode can be utilized, and the system's modularity is preserved. The design of the CSI and its dc-link inductor and other passive components has been well-studied in the literature. Typical sizes generally range from 0.5 to 0.8 per unit (pu) for the L_{dc}, 0.3– 0.6 pu for C_f, and 0.1–0.15 pu for L_f with a switching frequency of several hundred hertz.

2.3 Control Strategy

The control scheme for the proposed system is presented in Fig. 2-4. On the grid side, a conventional grid-tied system controller is applied, capable of active (dc-link current) and reactive power control. A conventional control scheme can be applied to the system [63].

On the battery side, each battery pack module has an independent control that checks the SoC of the battery to determine its operational condition. If SoC exceeds the threshold, the switch Q_i's gate signal (d_i) is on, and the battery supplies the output. On the other hand, when SoC goes below the threshold, d_i turns to zero, the battery will be disconnected, and the diode will bypass the module. The condition for reconnection of the battery could be varied depending on the requirements. For example, the batteries could be disconnected until fully charged or reconnected at certain lower SoC levels if necessary.

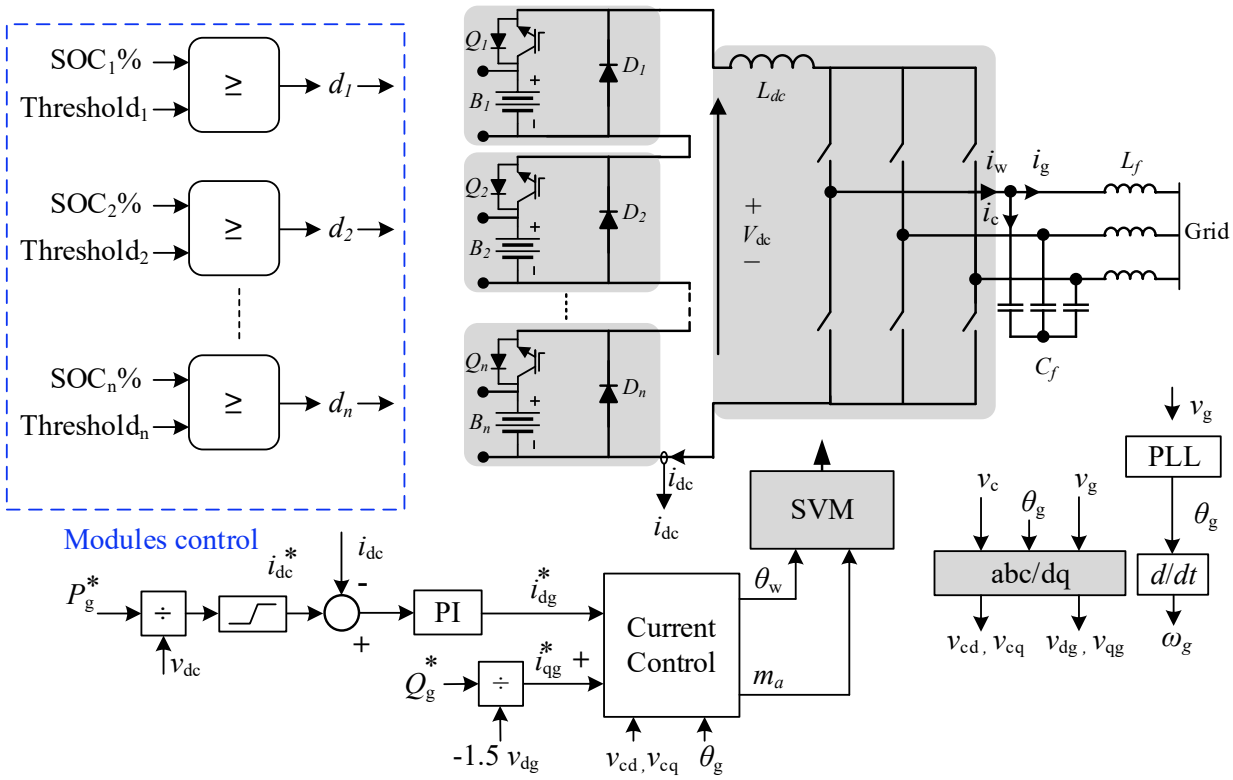

Fig. 2-4: Control strategy of the proposed grid-tied system.

The grid-tied CSI can operate either with a constant dc-link current reference (i_{dc}^{*}) or a constant output power reference (P_{g}^{*}). All active battery packs operate at a constant current determined by the grid-tied CSI. While working with a constant i_{dc}^{*}, when modules get bypassed, the modulation index (m_{a}) of the system changes, and the system continues to operate with a similar battery current with lower V_{dc} and output power. On the other hand, for constant P_{g}^{*}, when modules get bypassed, i_{dc}^{*} will increase to mitigate the reduction in the input power. The maximum allowed i_{dc}^{*} is determined based on the capability of the battery packs. The dc-link current is limited by the modules' maximum current capability. Under nominal operating conditions, m_{a} remains close to one. Importantly, the removal of the LFT is achieved through the use of a long string of low-voltage modules.

2.4 Comparison and Discussion

A comparison between the proposed converter and the existing one is presented in TABLE 2-1. The main criteria of comparison are:

LFT: Similar to CHB and MMC-based systems, the proposed converter does not require an LFT to connect to the MVAC grid. This is due to the use of a string of series-connected low-voltage battery modules and high-power MV (2.3-6.6 kV) CSI. CSI is a well-proven converter that can be scaled to higher voltages easily.

String length: A higher string length could have a negative effect on the performance of the inverter, as the weakest battery pack could limit the string. The proposed converter does not require a long string because it uses modular battery systems that can be bypassed.

Battery pack mismatches and power balancing scheme requirement: Unlike the conventional converters with short strings, such as CHB and MMC, the proposed converter inherently operates without power or voltage imbalance issues and is not limited by the weakest pack in the string. It

also eliminates the need for balancing strategies or topologies to manage varying SoCs across packs. This advantage stems from its variable dc-link voltage, enabling the system to seamlessly bypass depleted packs while maintaining operation.

TABLE 2-1. Comparison of different MVAC grid-tied inverters

Item	2LVSI [14]	2LVSI [55]	CHB [42]	MMC [52]	Proposed system
LFT requirement	Yes	Yes	No	No	No
String length	Single long	Short strings	Short strings	Short strings	Short strings
Power balancing requirement	-	Yes	Yes	Yes	No
Redundancy/overrating requirement	Yes	Yes	Yes	Yes	No

Failure protection (Redundant module/ module overrating): Failure protection can be implemented in CHB and MMC-based systems either by using redundant modules or module voltage overrating. Unlike conventional systems, the proposed system is protected against module failure or dc-link voltage reduction, as it can bypass all failed modules without negatively affecting the system's performance.

2.5 Simulation and Experimental Verification

Simulation and lab-scale experimental verifications are performed on the proposed system to validate its performance and effectiveness. The battery system can deliver up to 1.25 MW to the grid in simulation, while the maximum power of the experimental setup is 600 W.

2.5.1 Simulation Results

The proposed topology is simulated using MATLAB Simulink software. The specification of the system for the simulation is presented in TABLE 2-2.

The system is simulated with six series-connected modules, each containing batteries at different SoCs. The proposed converter operates in two control modes. In the first mode, constant current discharge (CCD) operation, a desired battery discharge current is set without consideration for the power delivered to the grid. Consequently, the system's output power varies based on the addition or elimination of modules. In the second mode of operation, the system works in constant power discharge (CPD) operation, where the system supplies fixed power to the grid. This mode is feasible only if the battery modules do not reach their rated current. However, when depleted batteries are bypassed, the system cannot deliver additional power, causing the battery's current to be limited to its rated value, I_{rated}.

Fig. 2-5 presents the simulation result of the proposed system in mode 1, with all battery modules discharging at I_{rated}. The initial SoCs of the modules are SoC_1 = 100%, SoC_2 = 80%, SoC_3 = 50%, SoC_4 = 40%, SoC_5 = 30%, and SoC_6 = 20%, demonstrating the step-by-step elimination of depleted batteries and its effect on the system. All batteries are disconnected when their SoC reaches 3%. Different minimum SoC thresholds can be selected based on the desired operating range of the batteries.

The figure shows that the batteries discharge and disconnect sequentially. Module voltages decrease gradually until the module is bypassed, at which point its output voltage drops to zero, reducing the voltage of the dc-link. The inverter adjusts the m_a and i_{w1} angle (θ_w) according to the required phase displacement and voltage gain. Since the system operates at I_{rated}, eliminating modules decreases the input power.

TABLE 2-2. Simulation parameters and components

Parameter/Component	Value
$V_{gL\text{-}L}$	4160 V
Number of battery modules (n)	6
Modules' rated voltage (V_{rated})	800 V
Modules' voltage range (V_m)	840-600 V
Modules' rated current (I_{rated})	250 A
L_{dc}	30 mH
C_f	100 μF
L_f	5 mH
CSI switching frequency	540 Hz
CSI modulation scheme	SVM

Fig. 2-6 presents the simulation results of the system operating in CPD mode, where one battery is fully discharged. The remaining batteries continue supporting the grid at a reduced power level of 500 kW. The battery SoCs are SoC_1 = 80%, SoC_2 = 60%, SoC_3 = 40%, SoC_4 = 30%, SoC_5 = 20%, and SoC_6 = 3%. At t_1 and t_2, two modules are bypassed, reducing the dc-link voltage. This, in turn, causes the current to rise to maintain constant output power. However, at t_4 and t_5, the system current has reached the rated current and cannot surpass it. As a result, the system transitions to CCD operation mode at the rated current, leading to a reduction in the output power.

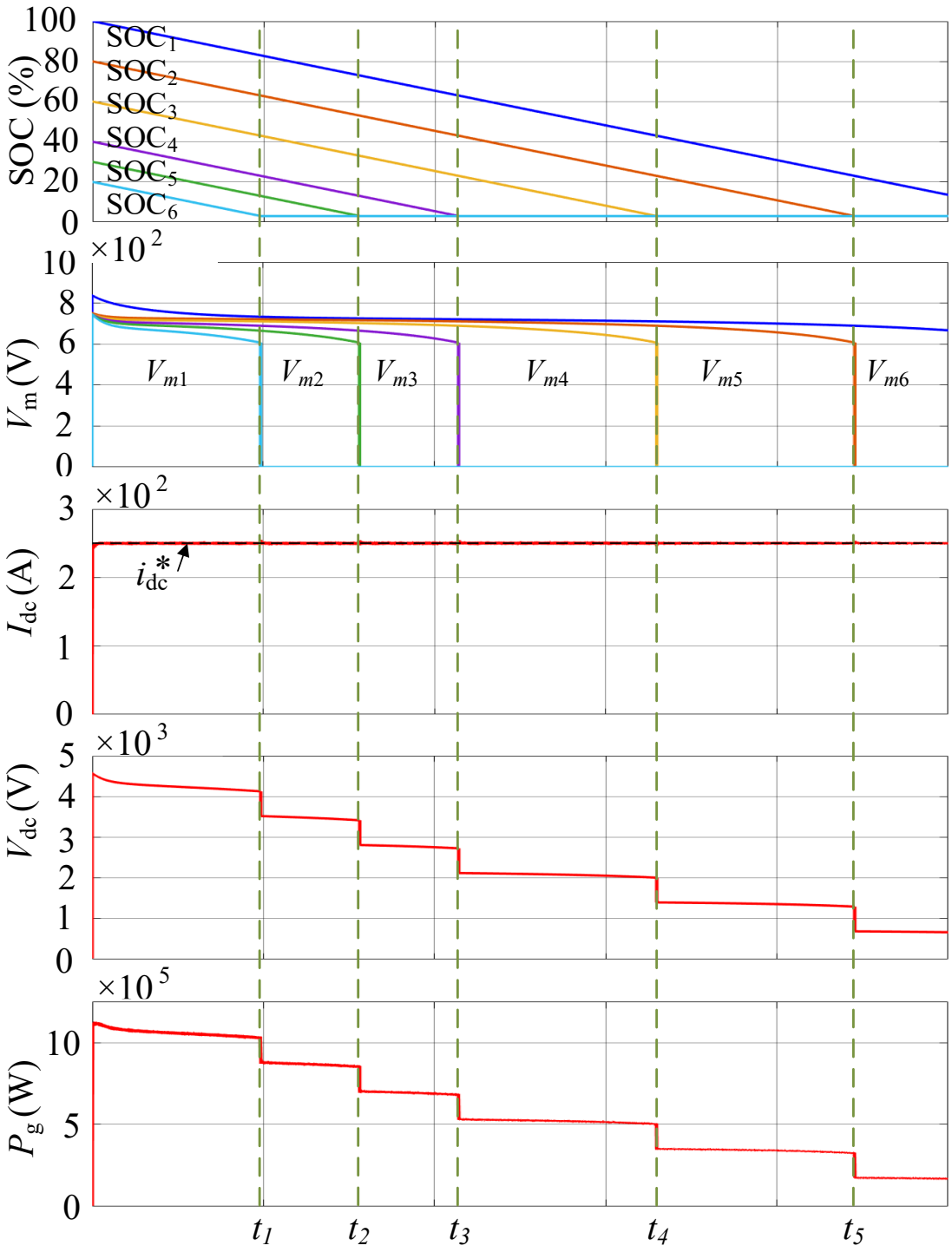

Fig. 2-5: CCD operation mode of the proposed system.

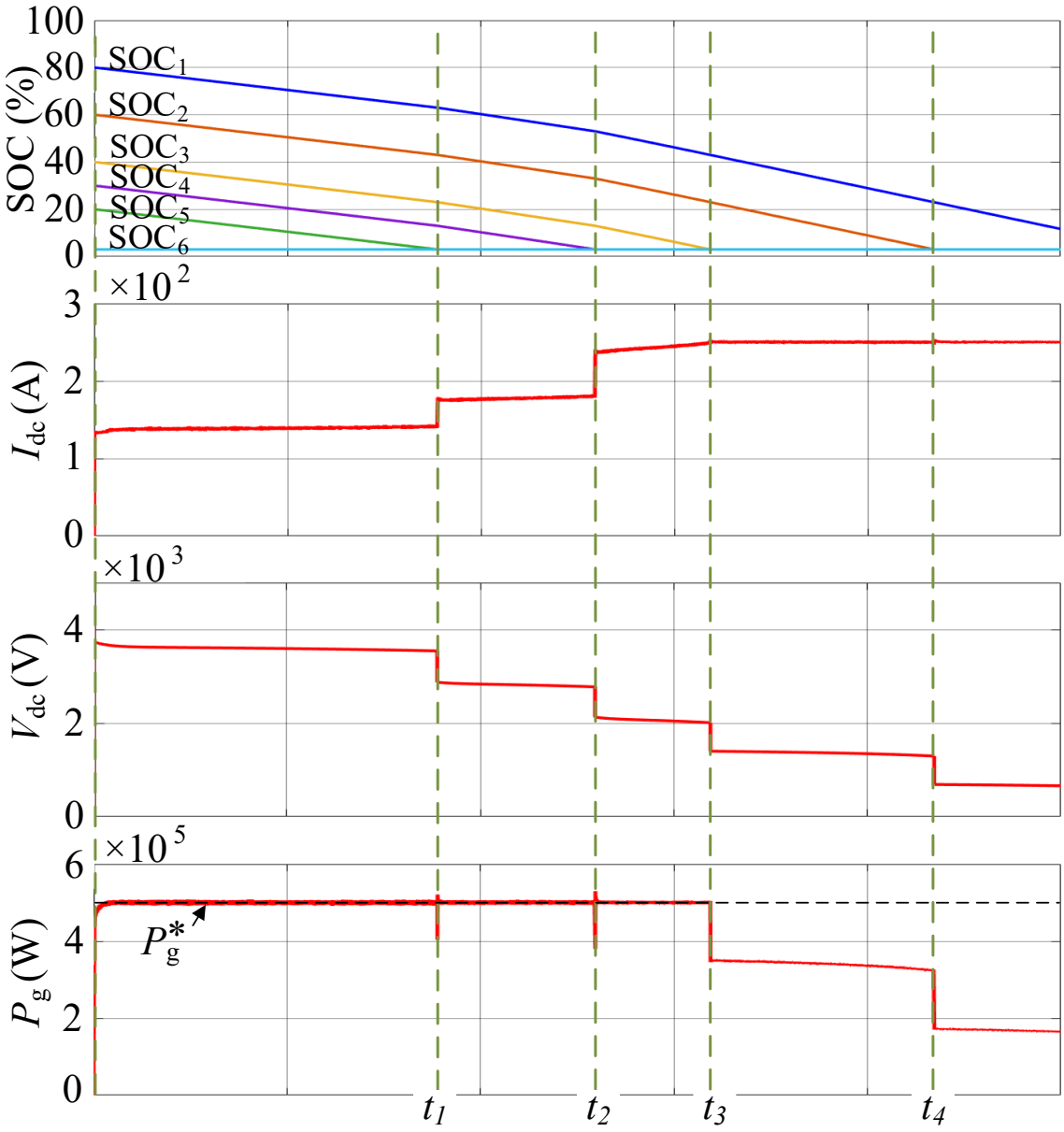

Fig. 2-6: CPD operation mode of the proposed system.

2.5.2 Experimental Verification

Experimental validation is conducted on a downscaled setup depicted in Fig. 2-7, which consists of both a schematic representation and a practical laboratory implementation. The system is

powered by a DC power supply with three independent outputs (DC_1, DC_2, and DC_3), each supplying a dedicated module. The output voltages of these modules (V_{m1}, V_{m2}, V_{m3}) are combined to form the total input voltage (V_{in}). On the output side, the CSI is connected to a resistive load (R_l) to emulate a practical load. The grid-connected operation of CSIs has been extensively studied in existing literature and, therefore, is not repeated in this work. An OPAL-RT real-time simulator is used to implement the system's control strategy. Additional details of the experimental system are provided in TABLE 2-3.

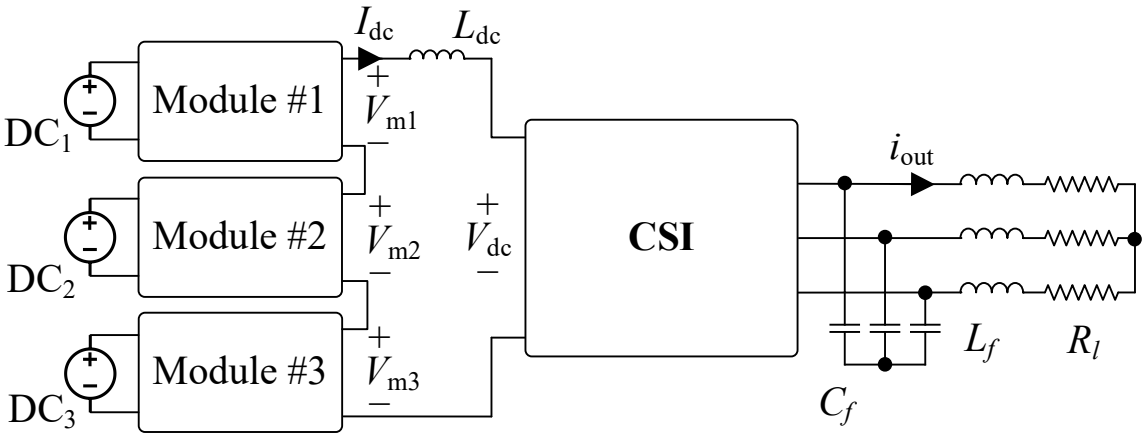

(a)

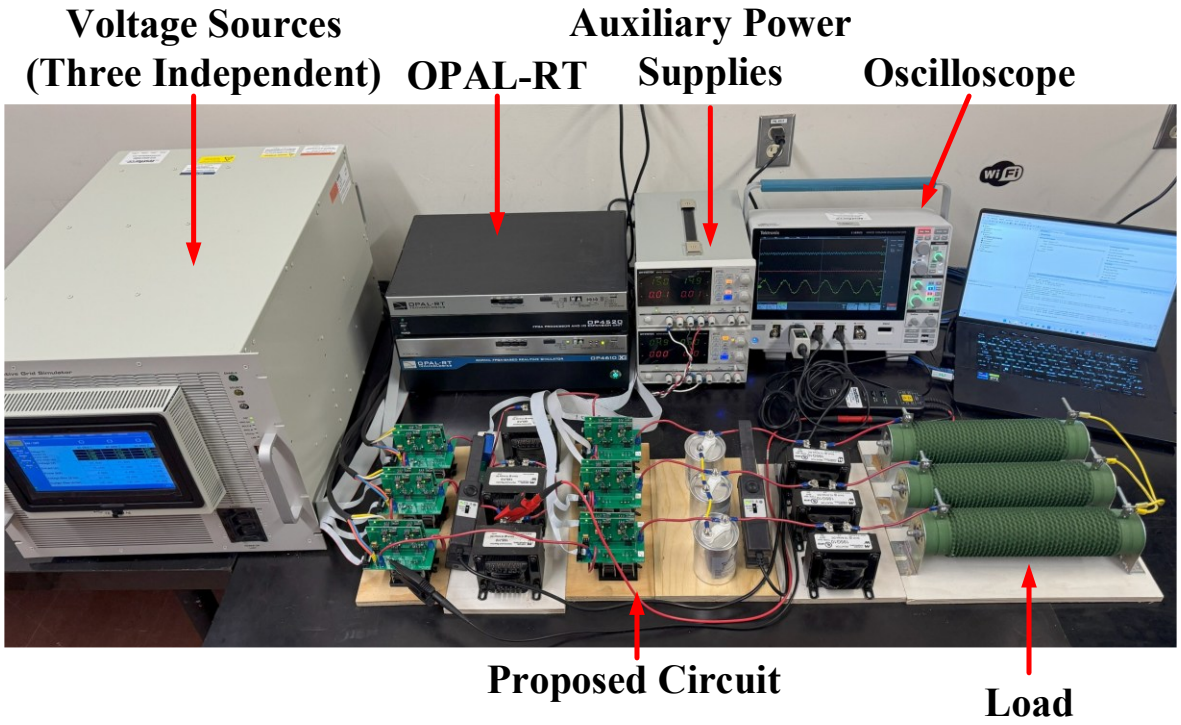

(b)

Fig. 2-7: Experimental setup. (a) Schematic diagram. (b) Experimental circuit.

TABLE 2-3. Experimental setup parameters and components

Parameter/Component	Value
Number of modules (n)	3
Modules' voltages (DC_1, DC_2, DC_3)	21 V
Modules' rated current (I_{rated})	10 A
L_{dc}	30 mH
C_f	100 μF
L_f	5 mH
CSI switching frequency	540 Hz
CSI modulation scheme	SVM
IGBT	IKW30N65ES5 650 V/ 30 A
R_l	21.2 Ω

Fig. 2-8 presents the experimental waveforms of the proposed system operating in CCD mode. In this mode, the input current is maintained at its rated value of 10 A. Modules #1 and #2 transition between bypass and active modes sequentially, simulating the system's response when batteries are temporarily disconnected due to a low SoC or a fault condition, and subsequently, reenter operation once recharged. The voltages of the modules are represented as V_{m1}, V_{m2}, V_{m3}. The waveforms show that as the modules are bypassed, V_{dc} decreases accordingly. Since the system operates at the constant rated current, the input voltage and power reductions are reflected in a corresponding decrease in power output.

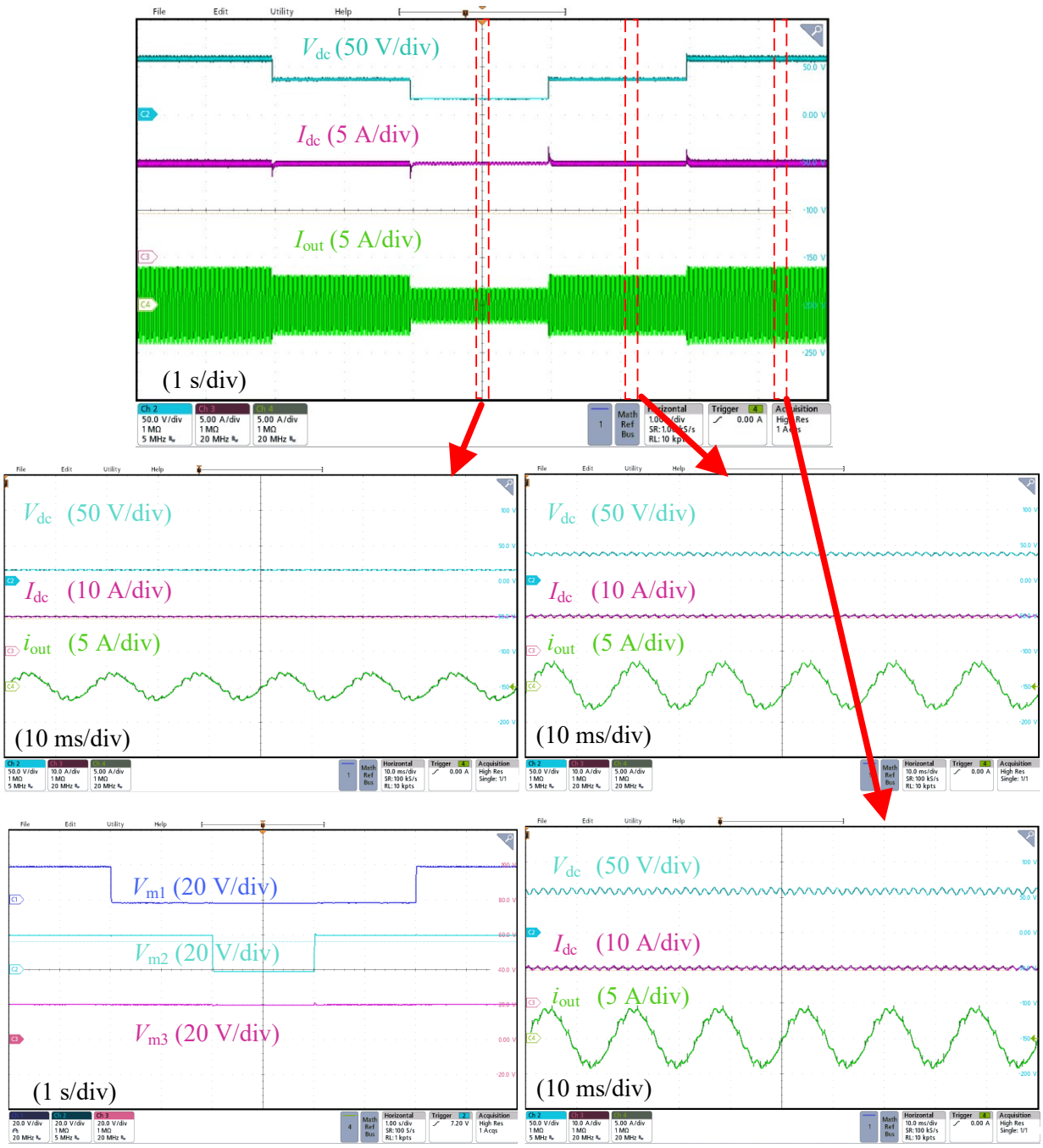

Fig. 2-8: Experimental waveform of the proposed system in CCD mode.

Fig. 2-9 presents the experimental waveforms of the system operating in CPD mode. In this mode, the system maintains a constant input power by adjusting the input current based on the number of active modules. Initially, the input current remains low with all the modules in active

mode. As the first module switches to bypass mode, followed by the second, the current through the remaining active modules increases. When only the last module remains active, its input current reaches the maximum limit while the required input power is sustained.

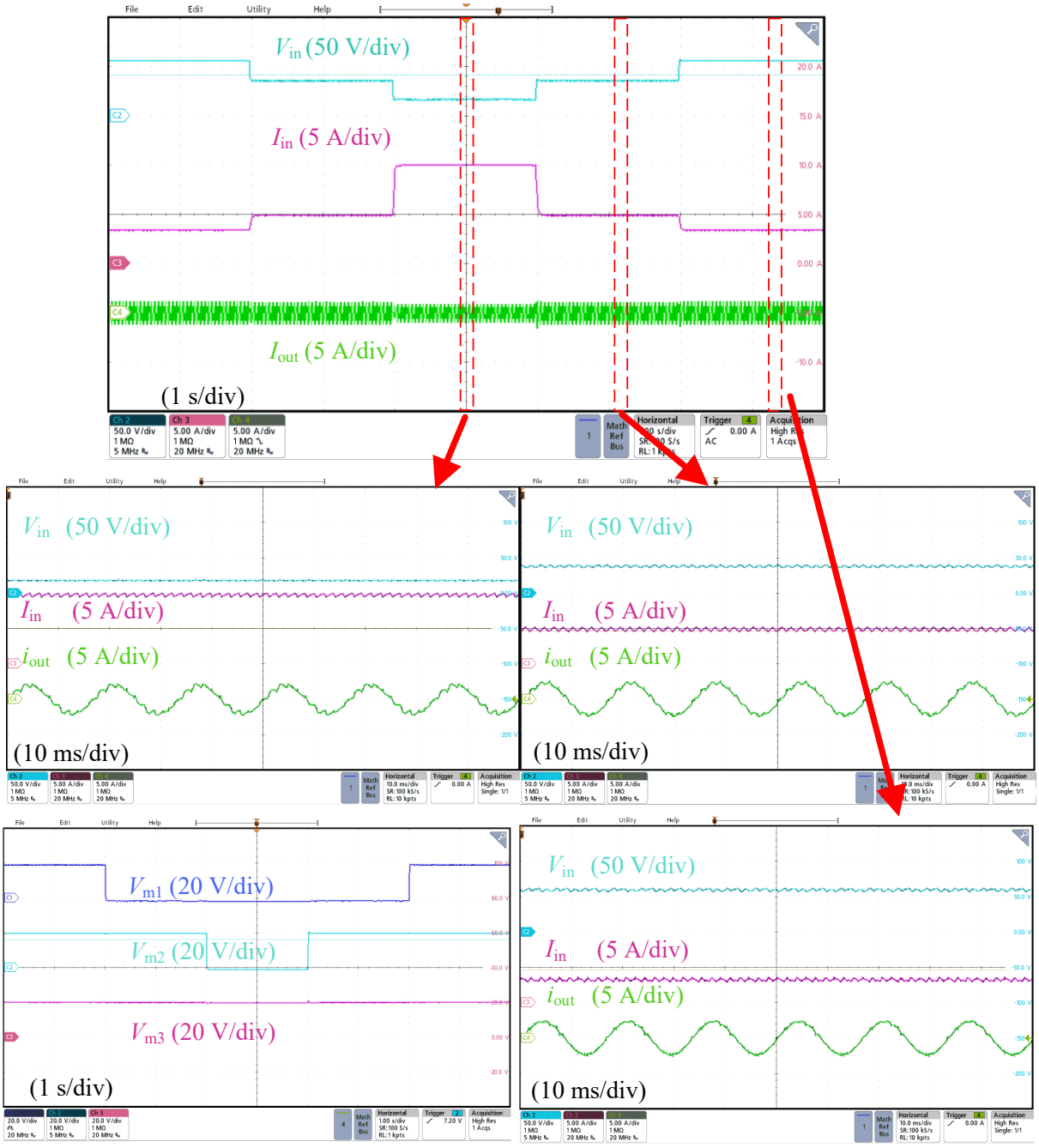

Fig. 2-9: Experimental waveform of the proposed system in CPD mode.

2.6 Chapter Summary

In this chapter, a CSI-based BESS was proposed for the grid integration of high-power RESs. By utilizing a string of modular low-voltage battery packs, the design eliminates the need for an LFT. This enables direct connection to MVAC grid levels while reducing system bulk and cost. Battery packs can be bypassed in the event of a fault or depletion without disrupting system operation. The proposed design eliminates the need for balancing controllers or circuits using the variable dc-link feature of CSI. Other key advantages of this design are its high scalability and inherent short-circuit protection. Both simulation and experimental results validate the converter's performance, demonstrating its effectiveness and the performance of the control scheme.

Chapter 3: A Current Source Rectifier-Based Modular Battery Charging System for BSSs

While chapter two focused on developing a CSI-based BESS topology for direct MVAC integration of RESs, the emphasis now shifts toward the modular battery charging systems, particularly for EV battery-swapping applications. Chapter three addresses key challenges of charger designs for BSSs interfaced with MVAC grids. Building on the modularity and transformerless operation explored previously, this chapter introduces a CSR-based charging system capable of reliable operation even under partial-load or low battery availability conditions, eliminating the need for overdesign or complex offline SoC balancing strategies. The proposed systems allow battery packs to be independently removed and replaced with empty ones without operational issues. Also, a two-stage control strategy is proposed that enables flexible constant current (CC) – constant voltage (CV) charging, supports pulsed current operation, and ensures stable performance under dynamic load conditions.

The chapter then presents the operating principle of the proposed CSR-based BSS battery charging station, along with key design considerations. Simulation results are provided to evaluate system performance under various operating conditions, and experimental validation is conducted to confirm the feasibility of the approach.

3.1 Principle of Operation

The proposed CSR-based BSS system is presented in Fig. 3-1. It consists of an MVAC grid-tied CSR and multiple series-connected battery charging modules. The CSR includes an LC filter on the input, six reverse blocking switches implemented using SCGTs, and an L_{dc}. Series-connected

switches are used to evenly distribute voltage stress across devices during MVAC grid operation. The CSR provides inherent short-circuit protection, low voltage rise rates, and grid-friendly waveforms due to its near sinusoidal input current.

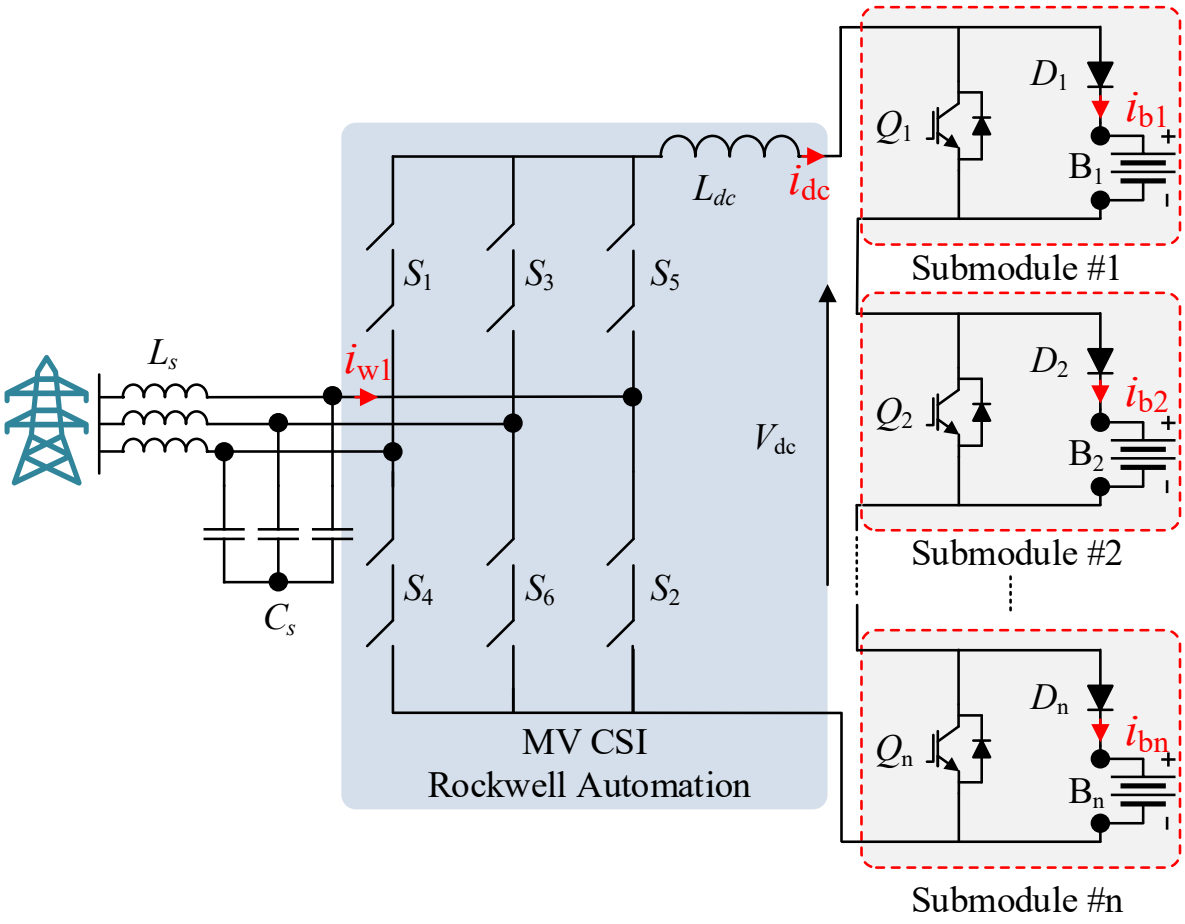

Fig. 3-1: Proposed BSS charger system.

CSR has wide applications in high-power and medium-voltage applications and can be utilized in the proposed system. MV CSRs are well-established industrial solutions for high-power medium-voltage applications in the 2.3–6.6 kV range, typically handling power levels from 1 MW to 4 MW. Industrial-grade implementations are already available; for instance, Rockwell Automation Canada offers a CSR-based drive topology that employs four switches per leg (two

per arm) for 4.16 kV and six switches per leg for 6.6 kV grid applications, demonstrating the practicality and scalability of such designs [62].

In contrast to voltage source rectifiers, which operate in boost mode, CSR is a buck-type rectifier that reduces the dc output voltage. V_{dc} of the rectifier is regulated through two techniques: varying the m_a or adjusting α between the grid voltage and i_{w1}. V_{dc} can be calculated as follows:

$$V_{\mathrm{dc}} = 3\sqrt{2}V_{rms}m_{\mathrm{a}}\cos\alpha \tag{3-1}$$

Therefore, the output voltage of the CSR can be reduced as the number of charging batteries plummets.

Each charging module comprises a battery pack (B_{n}) in series with a diode (D_{i}) and a parallel bypass IGBT (Q_{i}). An additional inductor is not required, as the CSR provides a smooth and continuous current to the modules. Due to the modular configuration, the total system voltage is distributed across multiple modules, significantly reducing voltage stress on individual components. As a result, low-voltage switches and diodes can be used within each module. The proposed system offers significant design flexibility. Using a stacked configuration of low-voltage modules eliminates the need for an LFT.

After a depleted battery is inserted into the charging module, Q_i turns off, D_{i} conducts, and the battery begins charging through the dc-link current. This process continues until the battery reaches the desired SoC. Then, Q_{i} turns on, D_{i} turns off, and the battery is bypassed, thereby stopping the charging process. As a result, the battery can be disconnected. Each time a battery is added or removed from the chain of series-connected batteries, V_{dc} adjusts accordingly. However, the dc-link current remains constant. Consequently, no offline balancing strategy or overdesign is required even when the number of charging batteries is low. The two modes of operation are illustrated in Fig. 3-2.

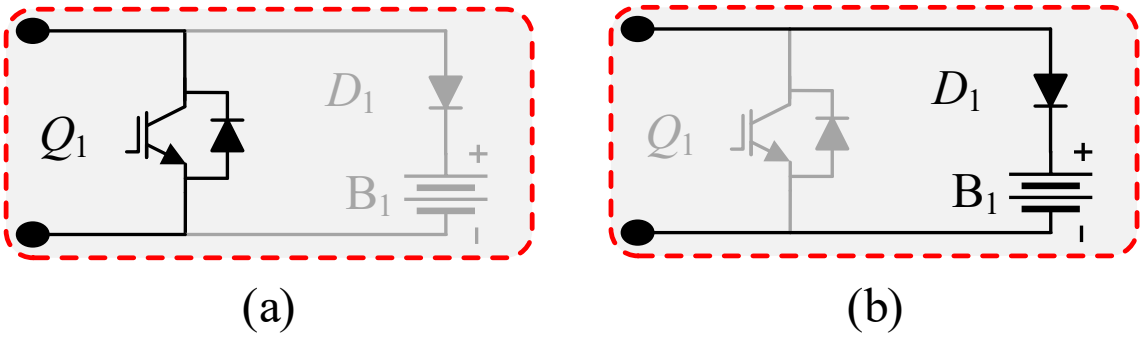

Fig. 3-2: Module modes of operation. (a) Bypass. (b) Active.

Each module's Q_i can also operate with a variable duty cycle ranging from 0 to 1, enabling buck-mode regulation of the charging current. By modulating the duty cycle of Q_i, the charging current can be precisely adjusted to deliver a controlled pulsed current to each battery. This enables independent, variable-current charging across all modules. Pulsed-current charging has been demonstrated to enhance battery lifespan and can be implemented using a range of switching frequencies [12].

3.2 Design Considerations

Considering a maximum of $m_{a,} = 1$, the maximum voltage allowed on the dc-link, $V_{\text{dc\_max}} = \sqrt{3/2}V_{\text{LL}}$. In this way, the buck-type operation of the CSR ensures system functionality even as the number of charging batteries decreases. The CSR in this study is designed for a 1.5 MW, 4160 V grid-connected application. The rated number of series-connected batteries is constrained by the maximum V_{dc} voltage CSR allows. The CSR requires series-connected switches capable of withstanding the grid voltage, which depends on the switch type and voltage rating. For instance, in a 4160 V grid, assuming 6.5 kV-rated SGCTs are used, a minimum of four devices in series per leg (i.e., two per arm) is required to ensure sufficient voltage-blocking capability and design margin. In high power medium voltage CSRs, L_f is in the range of 0.1-0.15 pu, and C_f is in the

range of 0.3-0.6 pu. Also, L_{dc} is in the range of 0.5 to 0.8 pu to reduce the current ripple to an acceptable range (less than 0.15%) [62]. The IGBT and diode of each module must withstand the L_{dc} current and battery voltages; as a result, for systems using typical 800V Li-ion batteries, 1200V semiconductors can be employed. Under these conditions, a maximum of six series-connected modules can be connected to the dc-link.

3.3 Control Strategy

A control scheme is designed for the proposed system, as presented in Fig. 3-3. The proposed control scheme consists of two parts. The first part (Fig. 3-3(a)) regulates i_{dc} and the input reactive power, using m_a and α. i_{dc} is set based on the rated current required by the charging batteries. The phase angle is compensated to correct the displacement introduced by the filter. Gate signals are produced using the space vector modulation (SVM) algorithm. It is worth noting that, under rated operating conditions, the modulation index approaches unity. The elimination of the LFT is not achieved by reducing m_a but rather by employing a long stack of low-voltage modules.

Battery current control for each module is shown in Fig. 3-3(b). The module-level control system consists of two stages. Initially, the batteries are charged in constant current (CC) mode until their voltage reaches the nominal battery voltage. The reference current for each battery (I_{Bi}^{*}) is compared with the battery current (I_{Bi}). Thus, the control system operates in three modes.

- If $I_{Bi}^{*} = i_{dc}$, then Q_i will be constantly OFF, and full current will flow through the battery.
- If I_{Bi} is zero, Q_i will be constantly ON, disconnecting the battery from the charging loop.
- If $0 < I_{Bi} < i_{dc}$, then a PI controller is used to regulate the current.

A slew-rate limiter is incorporated into the control loop to limit the rate at which the battery current reference changes, thereby preventing the introduction of large transients into the dc-link

current from the fast removal of batteries. Since the total dc-link voltage changes with each battery insertion or removal, the controller output must be updated accordingly. Once the battery voltage reaches its nominal value, the controller transitions to CV mode. In this mode, an outer voltage control loop regulates the battery voltage and generates a current reference, which is then tracked by the inner current control loop.

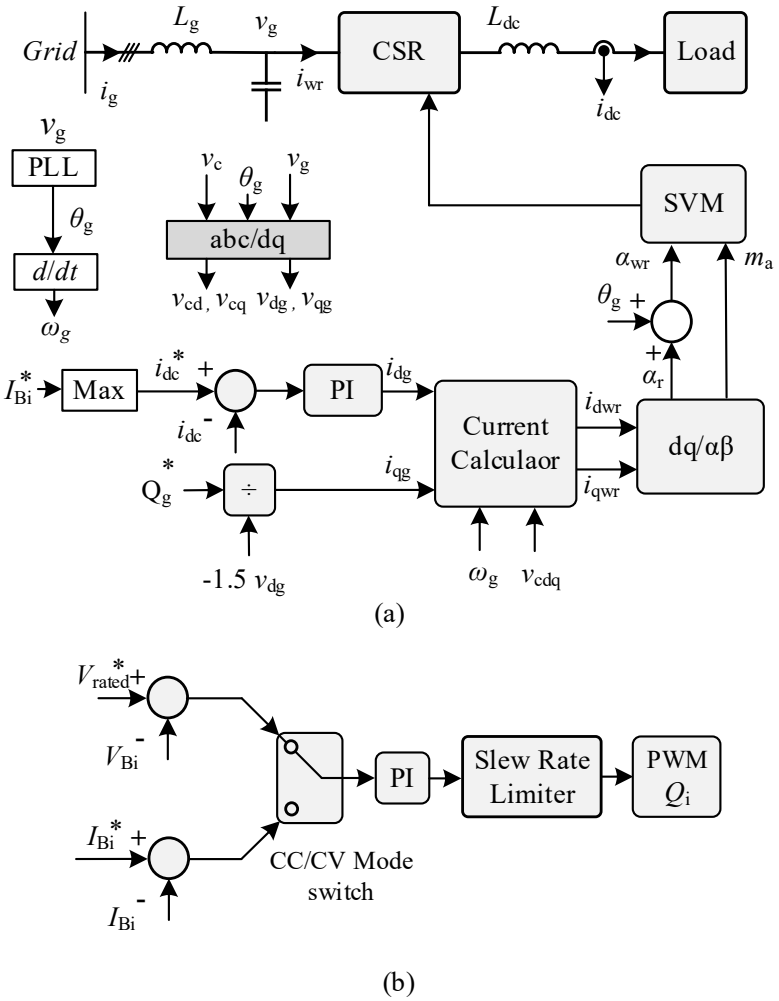

Fig. 3-3: Control scheme of the proposed system. (a) Grid-side control. (b) Module-level control.

3.4 Comparison and Discussion

The proposed CSR-based BSS system significantly improves several key aspects of conventional and state-of-the-art topologies as presented in TABLE 3-1. Conventional systems (Fig. 1-3) rely on LFTs and low-voltage distribution, resulting in bulky designs and high current ratings. Input-parallel (Fig. 1-10(a)) and input-series (Fig. 1-10 (b)) BSS structures enable direct MVDC connection, eliminating the need for LFTs. However, in the parallel configuration, each converter must handle a high step-down ratio, leading to elevated voltage stress. In contrast, the series configuration is susceptible to voltage imbalance when modules are bypassed due to battery removal or mismatch. These challenges require significant overdesign in both systems to ensure safe and reliable operation.

Offline SoC balancing via energy circulation proposed in the two-mode BSS system (Fig. 1-10(c)) attempts to solve the overdesign issue. Still, it accelerates battery aging due to redundant charge-discharge cycles. CHB and MMC-based systems provide modularity and reduced switch stress but are also prone to voltage imbalance when modules are removed, which compromises system reliability. The MMC-based BSS system presented in [61] (Fig. 1-10(d)) also relies on offline balancing. The proposed system eliminates the need for LFTs, supports independent connection and disconnection of batteries, avoids both overdesign and offline SoC balancing requirements with always-online operation, and offers inherent short-circuit protection and grid-friendly sinusoidal grid current.

TABLE 3-1. Comparison of different MVAC-Tied battery charging systems

Item	VSR [13]	VSR [17]	Two-mode VSR [58]	MMC-based [61]	Proposed system
LFT requirement	Yes	No	No	No	No
Current rating	High	Low	Low	Low	Low
Offline balancing requirement	No	No	Yes	Yes	No
Redundancy/overrating requirement	No	Yes	Yes	Yes	No

3.5 Simulation and Experimental Verification

The proposed system is evaluated through simulation in MATLAB/Simulink and validated using a lab-scale experimental prototype to confirm its functionality and performance. In the simulation, the battery system is capable of absorbing up to 1.5 MW from the grid, whereas the experimental setup achieves a maximum power intake of 450 W. The complete system specifications are provided in TABLE 3-2.

3.5.1 Simulation Results

The proposed system is simulated based on the design procedure described in Section II.B with six series-connected charger modules, each charging a battery. The initial SoC values of batteries B_1 through B_6 are set to 80%, 70%, 60%, 20%, 10%, and 0%, respectively. Although all batteries have the same capacity, the nominal charging current of the last battery is limited to half that of the others (150A). Each battery is charged to 98% SOC before being disconnected from the series string. Simulated waveforms of the proposed system are presented in Fig. 3-4.

TABLE 3-2. Simulation and experimental parameters

Parameter/ Component	Simulation Value	Experimental Value
V_{gLL}	4160 V/ 60 Hz	60 V/ 60 Hz
Number of modules (n)	6	3
Modules' voltage (V_{rated})	840-600 V (800 V)	15 V
Modules' rated current (I_{rated})	300 A	10 A
L_{dc}	30 mH	30 mH
C_s	100 µF	100 µF
L_s	5 mH	5 mH
CSI switching frequency	1080 Hz	1080 Hz
CSI modulation scheme	SVM	SVM
Switch	SGCT	IKW30N65ES5 650 V/ 30 A

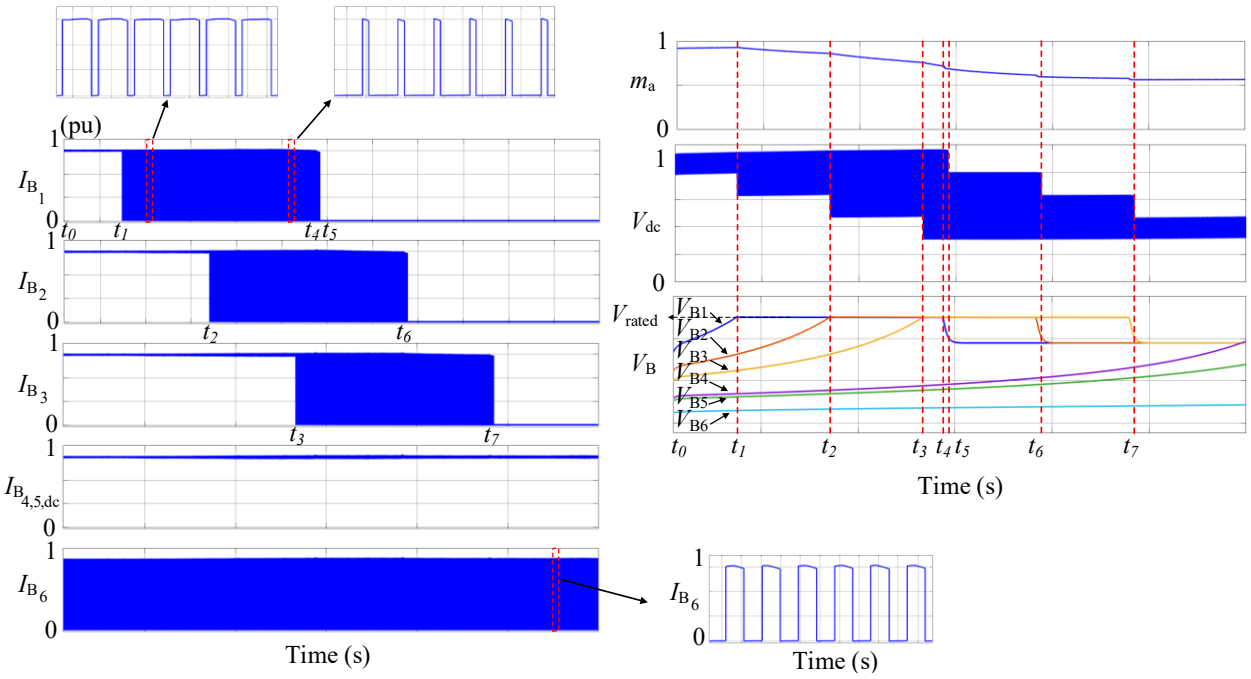

Fig. 3-4: Simulation results of the proposed system illustrating battery currents ($I_{B1, ..., B6}$), dc-link current (i_{dc}), modulation index (m_a), dc-link voltage (V_{dc}), and battery voltages ($V_{B1, ..., B6}$).

t_0-t_1: The simulation begins with all batteries operating in CC mode at the rated current (1 pu), while B_6 charges with a pulsed current of 0.5 pu due to its lower current reference until t_1. This demonstrates the system's ability to accommodate unequal charging currents across modules.

t_1-t_4: Once the voltages of B_1 reach the maximum charging voltage threshold (V_{rated}) at t_1, the controller transitions to CV mode, Q_i begins switching operation, and the battery receives.

t_4-t_5: After reaching its final SoC, B_1 is disconnected from the charging path. To avoid sudden transients in the dc-link current, the slew-rate limiter gradually reduces the battery current to zero over the interval t_4 and t_5. The dc-link current remains constant throughout the operation, as using a slew-rate limiter effectively prevents abrupt changes in load conditions that could otherwise result in overcurrent.

B_2 and B_3 follow the same sequence between t_2-t_6 and t_3-t_7, respectively, as they switch to CV mode upon reaching the voltage limit, receive pulsed current, and disconnect once their SoC targets are met. I_{B4} and I_{B5} are similar to i_{dc} as the corresponding batteries are still in CC mode of operation. This simulation scenario demonstrates the system's ability to operate under non-uniform battery conditions and dynamic events, including varying initial SOC levels and unequal current references, without compromising stability or requiring additional coordination mechanisms.

The simulation results confirm that the proposed system eliminates the need for offline SoC balancing, even when the number of active batteries is low. CSR-based topology dynamically adjusts the dc-link voltage to match the number of connected modules, and it has been verified that the system continues to operate with a low number of actively charging batteries. It can be observed that the system maintains a high modulation index when all modules are active, with a gradual reduction only as modules are bypassed and the resulting V_{dc} decreases.

3.5.2 Experimental Verification

Experimental tests were conducted on a lab-scale prototype of the proposed system. The implemented circuit and hardware setup are shown in Fig. 3-5. The experimental platform consists of a grid simulator, a CSR, and three charger modules connected to bidirectional independent dc sources (DC_1, DC_2, DC_3). The system's control strategy is implemented using an OPAL-RT real-time simulator.

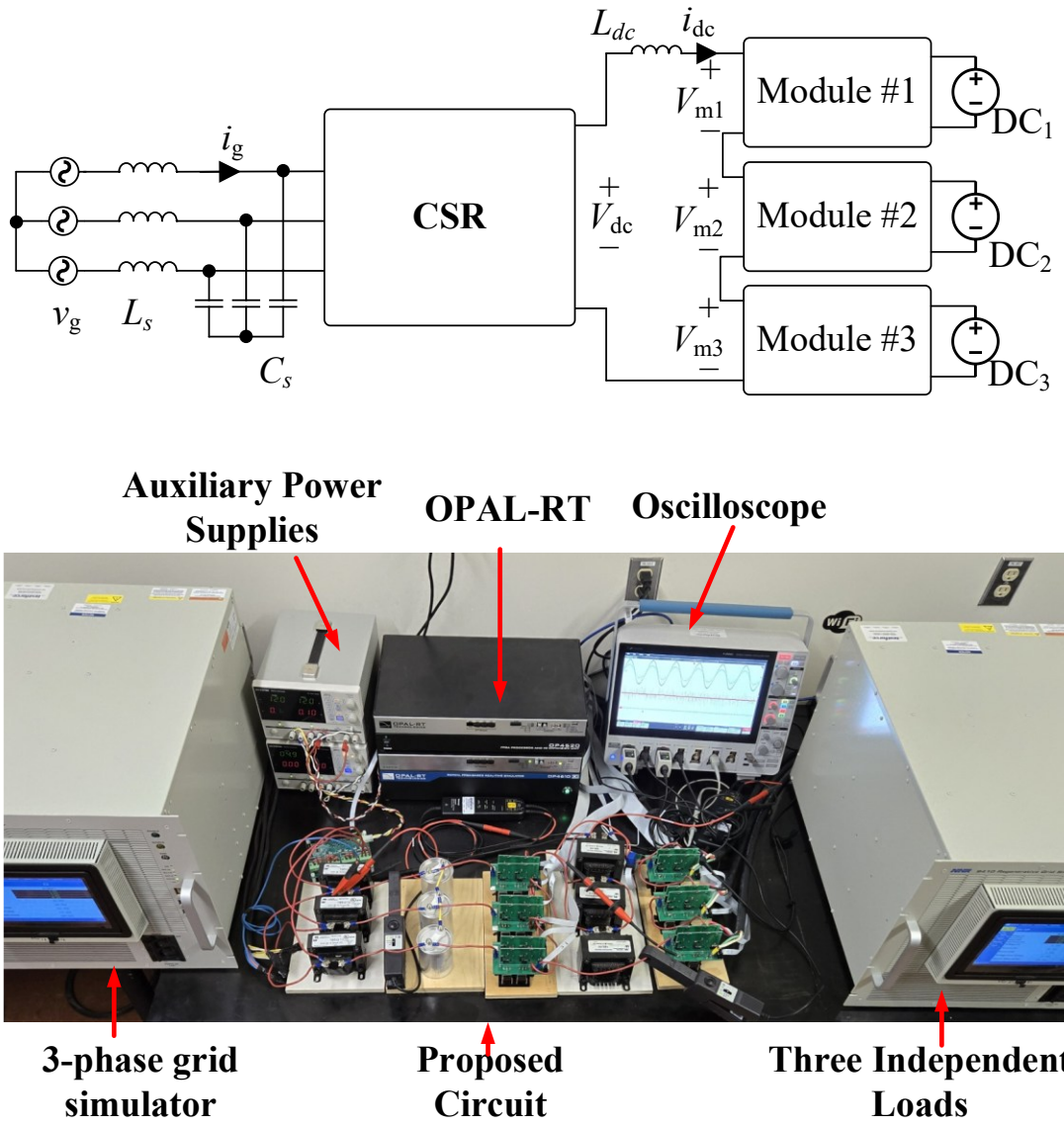

Fig. 3-5: Experimental setup.

Fig. 3-6 presents the experimental waveforms of the proposed system operating under various stages of CC and CV charging modes with different numbers of active modules. The waveforms include the grid voltage (v_g) and current (i_g), the dc-link voltage (V_{dc}) and current (i_{dc}), and also the current of the first battery (i_{DC1}).

Fig. 3-6 (a) shows the dynamic performance of the system during the full charging sequence of operation, while modules are in active mode with CC and CV operation and in bypassed mode. The details of each stage of the operations are further discussed in Fig. 3-6 (b) through Fig. 3-6 (f). Across all cases, i_g waveform closely follows v_g while the overall i_{dc} remains smooth, validating the system's operation.

Initially, all three modules operate in CC mode, each actively charging its corresponding dc sources via i_{dc} with the same current level, as shown in Fig. 3-6(b). This operation stage continues till t_1, demonstrating steady-state operation under full load conditions. The result confirms the effectiveness of the series-connected charging architecture in achieving a high V_{dc} and grid voltage without the need for an LFT, which aligns with the outlined design objectives.

As charging progresses, the first module transitions to CV mode at t_1, continuing until the load is fully charged and enters bypass mode at t_2. During this stage, i_{dc} remains constant. A pulsed charging scheme with a variable duty cycle is used to maintain CV regulation while gradually reducing the charging current. This approach produces pulsed current and voltage waveforms, enabling precise voltage regulation and preventing overvoltage during this charging phase. The average current gradually falls to zero as charging completes. Fig. 3-6(c) shows the CV operation with the bypass switch operating at 20% duty cycle, resulting in a battery current of 0.8 pu. As charging slows, the duty cycle increases, and the charging current decreases. Fig. 3-6(d) illustrates

the battery current dropping to 0.2 pu in the last charging stage before t_2. It is demonstrated that the system can flexibly modulate individual battery currents while maintaining a constant i_{dc}.

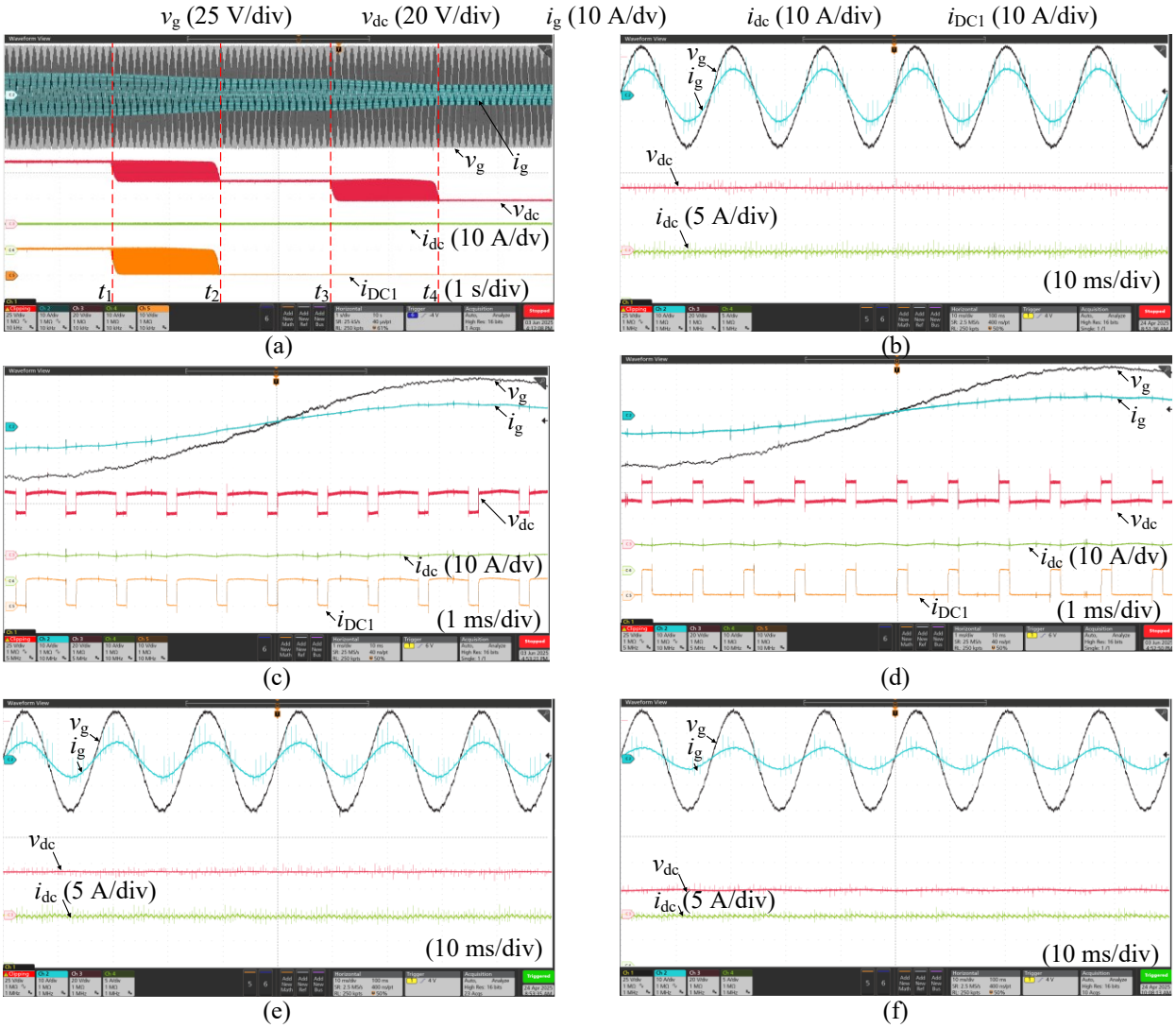

Fig. 3-6: Experimental waveforms for the system operation. (a) Dynamic operation. (b) Three active modules in CC mode. (c) Three active modules with two in CC mode and one in CV (i_{DC1} = 0.8 pu). (d) Three active modules with two in CC mode and one in CV (i_{DC1} = 0.2 pu). (e) Two active modules in CC mode. (f) One active module in CC mode.

After bypassing, the module output is disconnected, and the bypass switch is fully turned ON to ensure continuity. Fig. 3-6(e) shows the system with two modules in CC mode, following the bypassing of one module. The resulting reduction in the V_{dc} and i_g is observed accordingly, while the i_{dc} remains constant at 10A. Fig. 3-6(f) presents the most extreme case where only one module remains active. Despite the reduced module count and lower v_{dc}, the CSR continues to regulate current effectively, and the system remains stable. the remaining dc source continues charging. This verifies the system's ability to function without requiring offline balancing under a reduced module count under partial-load conditions.

In Fig. 3-7, one of the batteries is charged with a lower average current of 5 A by applying a pulsed current with a 50% duty cycle, while the other two are charging at full capacity. This figure showcases the system's ability to regulate and deliver a lower average battery charging current compared to the constant dc-link current, demonstrating its suitability for flexible and controlled charging scenarios.

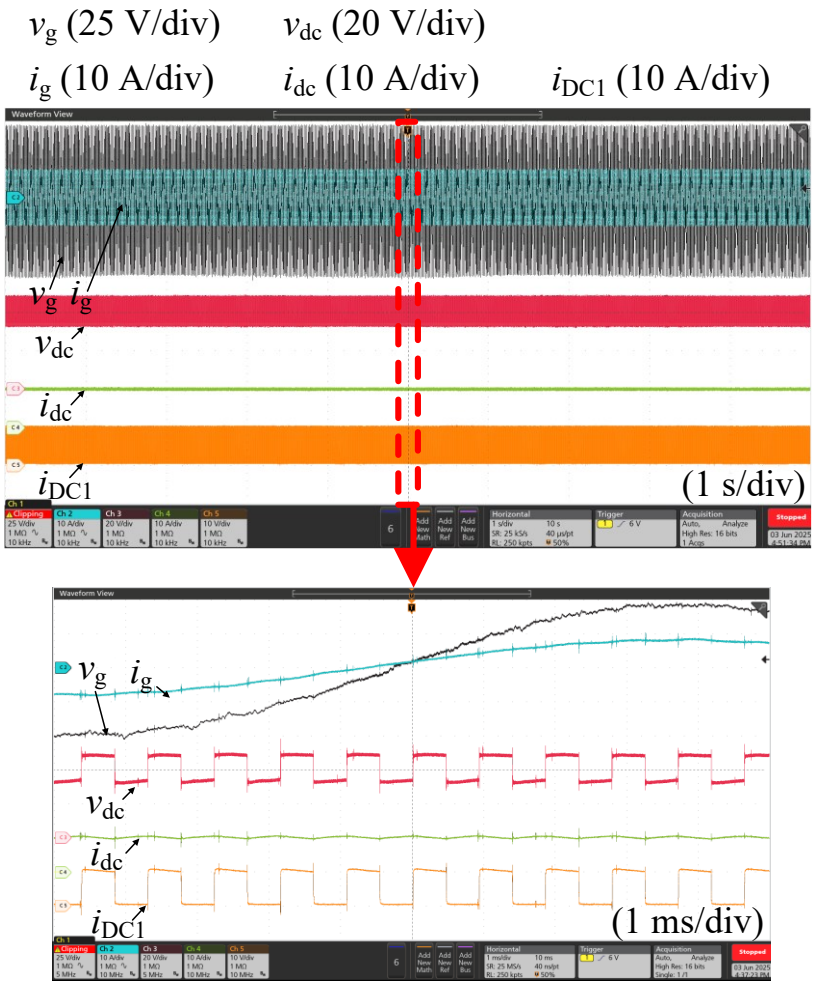

Fig. 3-7: Pulsed charging scenarios for a slower rate of charging.

3.6 Chapter Summary

A new CSR-based BSS charger system was proposed and validated for MVAC-connected applications. The topology addresses key limitations of conventional and state-of-the-art BSS designs, including the need for LFT and high current handling requirements, overdesign for voltage imbalance, or reliance on offline balancing during periods of low swapping demand. A two-part control system was developed to regulate both grid-side and module-level operation. On the grid side, the CSR modulates the dc-link current and reactive power. At the module level, a two-stage control scheme enables CC-CV charging and supports pulsed-current modulation, allowing precise current shaping for each battery. Simulation results and experimental tests confirm the system's ability to maintain a constant dc-link current during dynamic events such as module insertion, removal, and CC–CV mode transitions. These capabilities make the system a strong candidate for high-power battery swapping infrastructure that operates reliably under partial loading and non-uniform battery conditions.

Chapter 4: A Current Source Converter-Based Modular Battery Energy Storage System for Bidirectional Grid Integration

Chapter three introduced a modular CSR-based battery charging system for high-power BSS applications. The design eliminates the need for LFTs and addresses challenges such as overdesign, voltage imbalance, and offline SoC balancing requirements. A two-stage control scheme enabled flexible CC–CV charging and pulsed current operation, while maintaining reliable performance under partial-load and dynamic conditions.

From this basis, in this chapter, we introduced a bidirectional BESS converter based on a high-power medium-voltage current source converter (CSC), using series-connected battery modules. Operating with a variable dc-link voltage, the system maintains stable performance even under significant SoC imbalance or battery faults. It eliminates the need for redundancy, overrating, or complex balancing schemes. This architecture offers a robust and practical solution for SLB integration in grid-tied applications.

4.1 Principle of Operation

The proposed system is depicted in Fig. 4-1. It comprises two main parts, the battery-side modules and the grid-side converter. On the grid side, a high-power medium-voltage CSC is employed.

The CSC consists of a dc-side inductor to smooth the current flow, six reverse-blocking semiconductor switches, and an ac-side filter. CSC technology is well-established in industrial medium-voltage applications and is commonly used in systems dealing with high power levels.

Multiple devices are connected in series within each phase leg to satisfy medium-voltage requirements.

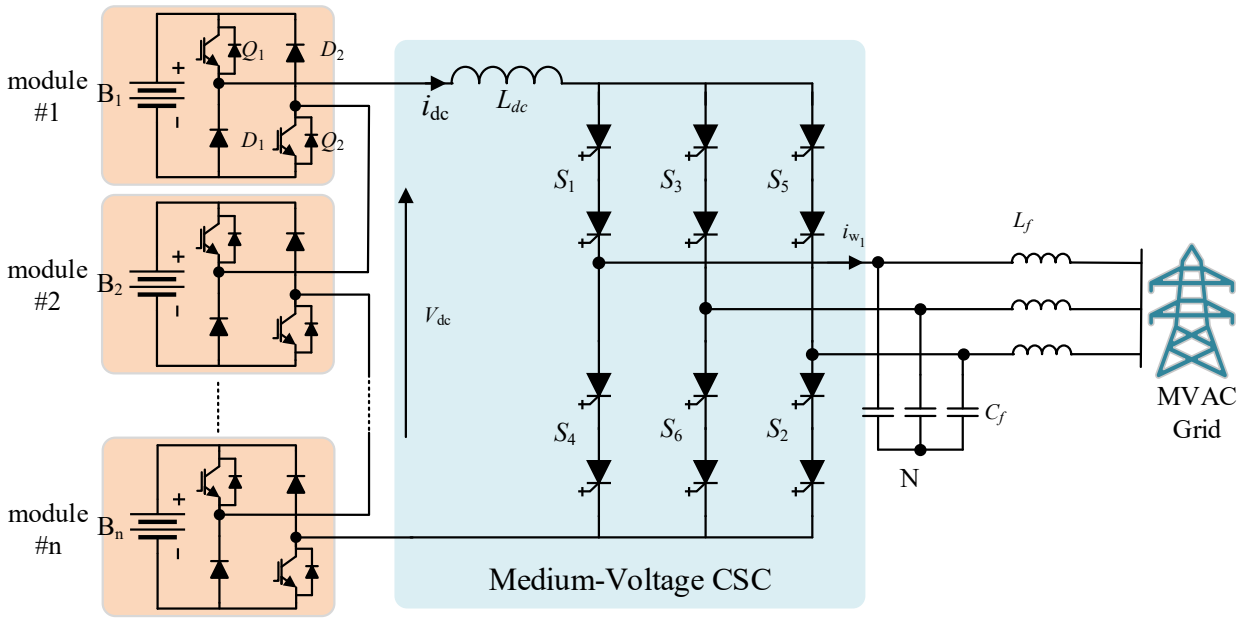

Fig. 4-1: Proposed modular CSC-based BESS.

The system supports bidirectional power flow with the MVAC grid, depending on the system's operating mode. During discharge mode, energy stored in the battery modules is transferred to the grid through the CSC. In charging mode, energy is absorbed from the grid and directed to the active battery modules for replenishment. Throughout operation, i_{dc} remains regulated, while V_{dc} varies with the number of connected modules. This current-controlled and variable-voltage operation enables continued functionality even when certain modules are bypassed due to faults or SoC limits.

On the battery side, several battery modules are connected in series to form V_{dc}. Each module includes an SLB connected to a bidirectional dc chopper, composed of two IGBT switches and two diodes. The dc chopper regulates both the magnitude and direction of the battery current. The

operating modes of the modules are illustrated in Fig. 4-2. Since i_{dc} always flows in a positive direction, all modes exhibit unidirectional current flow, and continuous current operation of CSC must be maintained.

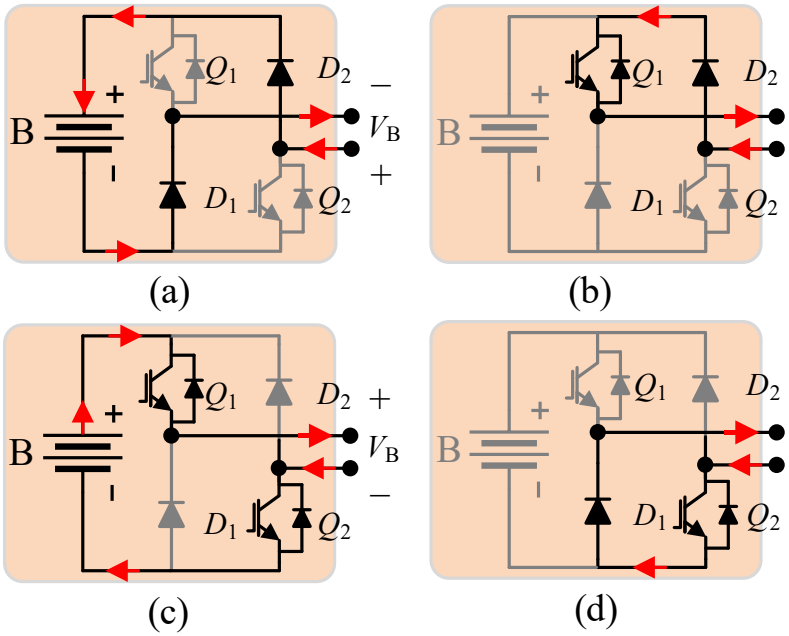

Fig. 4-2: Modes of operation of the dc chopper. (a) Discharging. (b) Bypass. (c) Charging. (d) Bypass.

The modules operate in four distinct modes, depending on the switching states of Q_1 and Q_2.

- In mode I, both switches are off, and diodes D_1 and D_2 conduct. The battery charges, and assuming ideal components, the module output voltage is equal to $-V_B$, as shown in Fig. 4-2(a).
- In mode II, Q_1 is on and Q_2 is off. Under this condition, D_1 is reverse-bias, and D_2 conducts. The module is in bypass mode with zero output voltage and no battery current, as shown in Fig. 4-2(b).

- In mode III, both switches are on, and the diodes are reverse-biased. The battery discharges, and the module output voltage equals V_B (Fig. 4-2(c)).
- Mode IV is similar to mode II, but Q_2 is on and Q_1 is off, resulting in current conduction through D_1 (Fig. 4-2(d)).

By increasing the number of series-connected battery modules, the total V_{dc} rises proportionally. This modular stacking approach enables the system to reach the required voltage levels for medium-voltage applications. As a result, medium-voltage CSC can interface directly with the MVAC grid without requiring an LFT.

4.2 Design Considerations

The proposed system supports bidirectional energy exchange with the MVAC grid, enabling both power injection through battery discharge into the grid and power absorption through battery charging from the grid, depending on operating conditions. Each battery module operates independently, and the system dynamically adapts to the number of active modules. Importantly, during either charging or discharging modes, individual modules may engage in charging or discharging based on their local SoC and control commands, enabling decentralized and flexible operation.

Two examples illustrating the operation of the proposed system in charging and discharging modes are presented in Fig. 4-3. In Fig. 4-3 (a), the system operates in discharging mode, where all active modules are discharging the batteries and contribute positive voltage to the overall V_{dc}, while one module is bypassed. in Fig. 4-3 (b), the system is in charging mode, with most modules charging the batteries, except one, which is bypassed. These cases highlight the system's ability to maintain continuous operation even when some modules are bypassed due to faults or SoC-related conditions, thanks to the variable nature of V_{dc} in CSC. As modules are removed from the string,

whether due to failures or early depletion/full charge, the CSC maintains power delivery by adapting to a lower modulation index. Nevertheless, the maximum power delivery may be reduced based on the power demand and the remaining battery capacity.

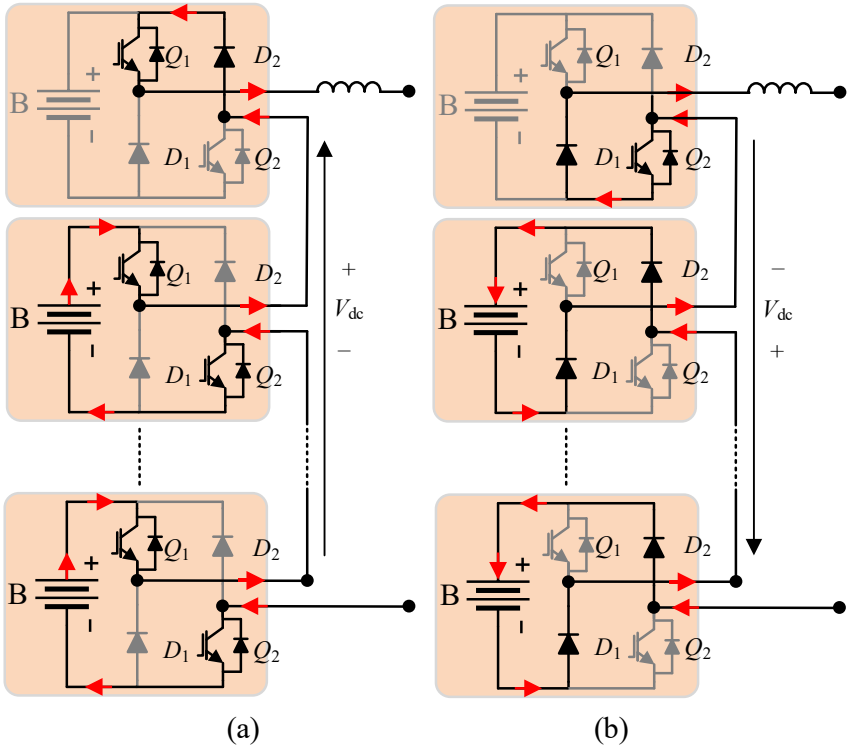

Fig. 4-3: System modes of operation. (a) Discharge. (b) Charge.

The proposed system remains operational as long as the total string voltage satisfies the following conditions:

$$V_{\mathrm{dc}} = 3\sqrt{2}V_{rms}m_{\mathrm{a}}\cos\alpha \tag{4-1}$$

m_{a} is equal to:

$$m_a = \frac{\sqrt{2}I_{\mathrm{w1}}}{i_{\mathrm{dc}}} \tag{4-2}$$

In the series-connected topology, V_{dc} is the sum of the voltages of the chopper modules, and thus it cannot surpass equation (4-1), considering m_{a} is less than one. V_{dc} becomes:

$$|V_{dc}| = \sum_{i=1}^{n} d_i . V_{Bi} \tag{4-3}$$

where d_i is the duty ratio of modules. This relation is valid in both charge and discharge operations based on the power-flow direction and the active switches.

This flexibility eliminates the need for complex balancing strategies and removes constraints typically imposed by SoC equalization requirements. As a result, the system operates reliably across a wide range of conditions without being limited by the performance of individual modules.

4.3 Control Strategy

A hierarchical control scheme is proposed for the coordinated operation of the proposed bidirectional modular BESS. The control scheme for the proposed system is illustrated in Fig. 4-4. The control objective is to regulate the dc-link voltage and current such that the power reference $\underline{P}_g^\star$ is met while maintaining safe operation of each battery module. The control structure operates over several steps as outlined next.

The control cycle begins by determining the power-flow direction. If $\underline{P_g}^\star$ is positive, the system enters the discharge or source mode, supplying power to the grid. If $\underline{P_g}^\star$ is negative, the system enters the charging or sink mode, absorbing power. This decision dictates which switches and modes of operation in the bidirectional choppers are active.

The duty cycles of both switches in the active module are set to:

$$d_i = \begin{cases} 1 & if\ P_g^* > 0 \\ 0 & if\ P_g^* < 0 \end{cases} \tag{4-4}$$

If the module is required to be bypassed, the duty cycles would be complementary, and either switch can be turned on. In sink mode, as the battery storage in each module depletes, the corresponding module transitions from active mode to bypass mode.

The dc-link voltage will be set to maximize the instantaneous voltage of the string. i_{dc} is regulated based on the desired output power, in which the discharging requirements of the battery are reflected. The corresponding string current is

$$i_{dc} = \frac{|P_g^*|}{V_{dc}} \tag{4-5}$$

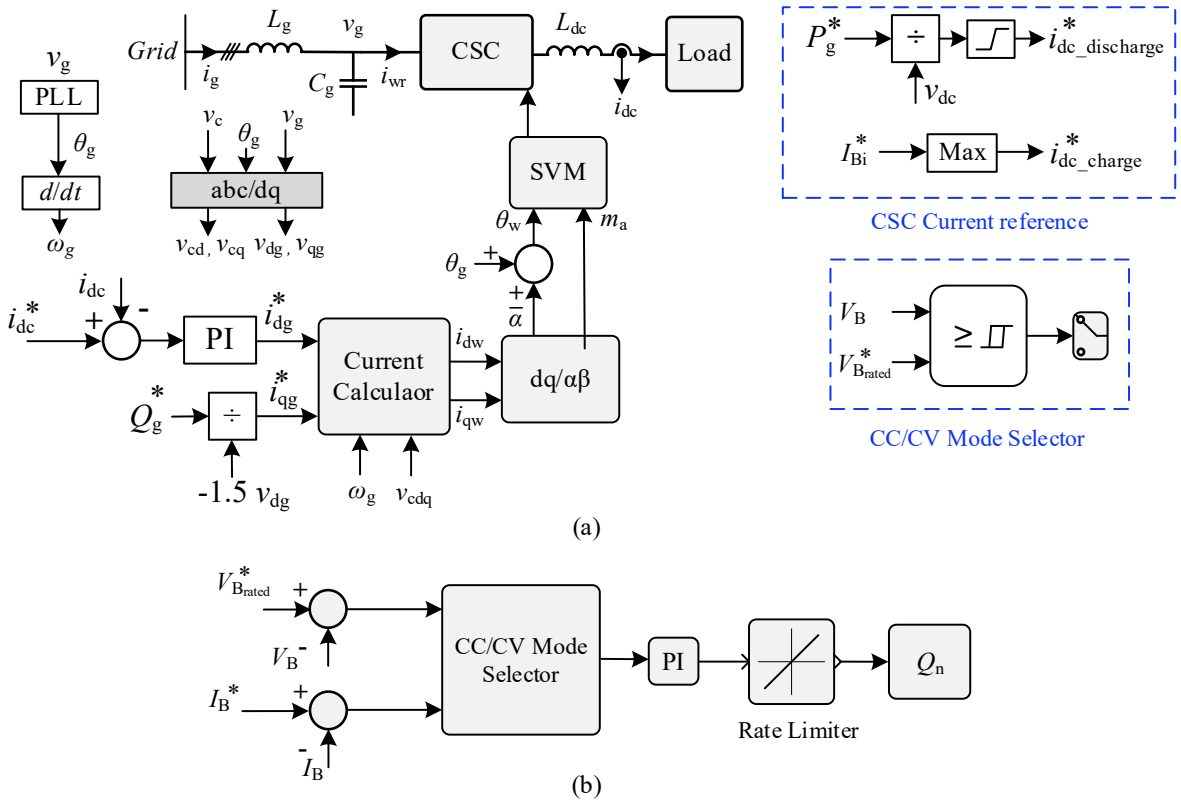

Fig. 4-4: Control strategy of the proposed system.

During battery charging, the modules operate in two sequential modes. Initially, while each cell voltage is below V_{rated}, every module is driven in CC mode. With charging currents equal to i_{dc},

or pulsed current charging based on the maximum safe charging current of the battery. The supervisory controller sets a common i_{dc}, and each module tracks the local reference with its inner current loop.

$$i_{Bi} = d_i . i_{dc} \tag{4-6}$$

As soon as the terminal voltage reaches V_{rated}, that module switches to CV mode. In CV mode, the module controller adjusts the duty cycle to hold the battery voltage constant. When all batteries transition to CV mode, batteries are charged through variable duty cycle PWM pulsed current charging to keep the battery voltage at nominal until fully charged. The dc-link current is steadily reduced to match the declining charge demand.

4.4 Comparison and Discussion

This section provides a comparative analysis of conventional and modular BESS configurations with respect to their scalability, fault tolerance, balancing requirements, and suitability for heterogeneous SLBs, as presented in TABLE 4-1.

Grid interface: Both modular-based systems and the proposed CSC architecture support transformerless integration with the MVAC grid, eliminating the need for bulky LFT used in conventional VSI-based BESSs.

Adaptability to battery heterogeneity: Adaptability is limited in centralized BESSs with LFT, where battery strings are connected in parallel to a common dc-link, which prevents individual control. Decentralized LFT-based BESSs solve this issue using decentralized rectifiers or additional dc-dc stages. In modular converters like CHB and MMC**,** battery heterogeneity leads to power imbalance between modules, requiring complex balancing strategies or hardware. The

weaker cells can be bypassed or throttled in the proposed system, and the power is redistributed to the rest of the modules. As a result, it provides adaptability to battery heterogeneity**.**

Balancing complexity: CHB and MMC-based topologies require complex balancing strategies, including ZSV injection and circulating current control. The proposed control strategies in the literature face limitations under extreme cases due to the power transfer boundaries of these systems. LFT-based and the proposed systems enable simpler control at the module level, making them more manageable in SLB applications.

Fault tolerance: In CHB and MMC systems, the failure of a single submodule can compromise the operation of the entire converter string unless redundancy is employed. The proposed system maintains operation even under module faults by supporting selective bypass.

TABLE 4-1. Comparison of different MVAC-tied BESS systems

Feature	Grid interface	Battery connection	Adaptability to heterogeneous cells	SoC balancing complexity	Impact of failed modules
Centralized dc-ac	LFT-based	Parallel strings	Low, packs must be matched	Not possible	Minimal (remove string)
Decentralized dc-ac	LFT-based	Single strings	High, independent control	None (independent)	Minimal, Isolated to the module
Decentralized dc–dc with a common dc-link	LFT-based	Single strings	High, independent control	None (independent)	Minimal Isolated to that module
Modular CHB / MMC	Direct MVAC	Single strings	Limited	High	String output degraded; redundancy needed
Proposed system	Direct MVAC	Single strings	High, variable dc-link	None	Minimal, bypasses faults

4.5 Simulation and Experimental Verification

The proposed system is validated through MATLAB/Simulink simulations and subsequently verified using a scaled experimental setup. TABLE 4-2 outlines the full set of system specifications applied.

The proposed system was simulated using batteries with heterogeneous capacities with different levels of SoC and depth of discharge as presented in TABLE 4-3.

TABLE 4-2. Simulation and experimental parameters

Parameter/ Component	**Simulation Value**	**Experimental Value**
V_{gLL}	4160 V/60 Hz	60 V/60 Hz
Number of modules (n)	6	3
Modules' voltage (V_{rated})	840-600 V (800 V)	15 V
Modules' rated current (I_{rated})	300 A	10 A
L_{dc}	30 mH	30 mH
C_s	100 μF	100 μF
L_s	5 mH	5 mH
CSI switching frequency	1080 Hz	1080 Hz
CSI modulation scheme	SVM	SVM
Switch	SGCT	IKW30N65ES5 650 V/30 A

TABLE 4-3. Simulation battery parameters

Module battery	Capacity (pu)	SoC range
B_1	0.375 pu	10%-90%
B_2	0.5 pu	10%-90%
B_3	0.625 pu	20%-80%
B_4	0.75 pu	30%-70%
B_5	0.875 pu	20%-80%
B_6	1 pu	3%-97%

4.5.1 Simulation Results

All batteries are considered depleted in charging mode and are charged from their minimum SoC. Similarly, in discharging mode, all batteries are considered full and are discharging for the maximum SoC level.

Discharge Mode:

The simulation results of the discharging mode are presented in Fig. 4-5 and Fig. 4-6. The simulation starts with all battery modules fully charged and operating in discharging mode at their rated current. Each module continues discharging until its SoC reaches the predefined minimum threshold, at which point the module is bypassed. As modules transition into bypass mode, V_{dc} decreases accordingly. The influence of the rate limiter is evident in the V_{dc} profile, which ensures a controlled reduction in output voltage and prevents transients. As a result, i_{dc} supplied to the grid remains unaffected during individual module disconnections.

Similarly, the simulation results for the charging mode are presented in Fig. 4-7 and Fig. 4-8. In the charging mode simulation, all battery modules begin at their initial SoC and charge at the rated current. As each module reaches its maximum SoC threshold, it is switched to bypass mode. The bypassing of modules leads to a gradual reduction in V_{dc}. The rate limiter effectively smooths the transition instances and achieves a smooth i_{dc}. CC to CV mode is implemented on batteries that achieve their rated voltage before being fully charged.

The simulation results show that the system can operate using heterogeneous batteries with variable capacity and SoC ranges. The simulation results also confirm that the proposed system eliminates the need for LFT and does not require complex balancing schemes.

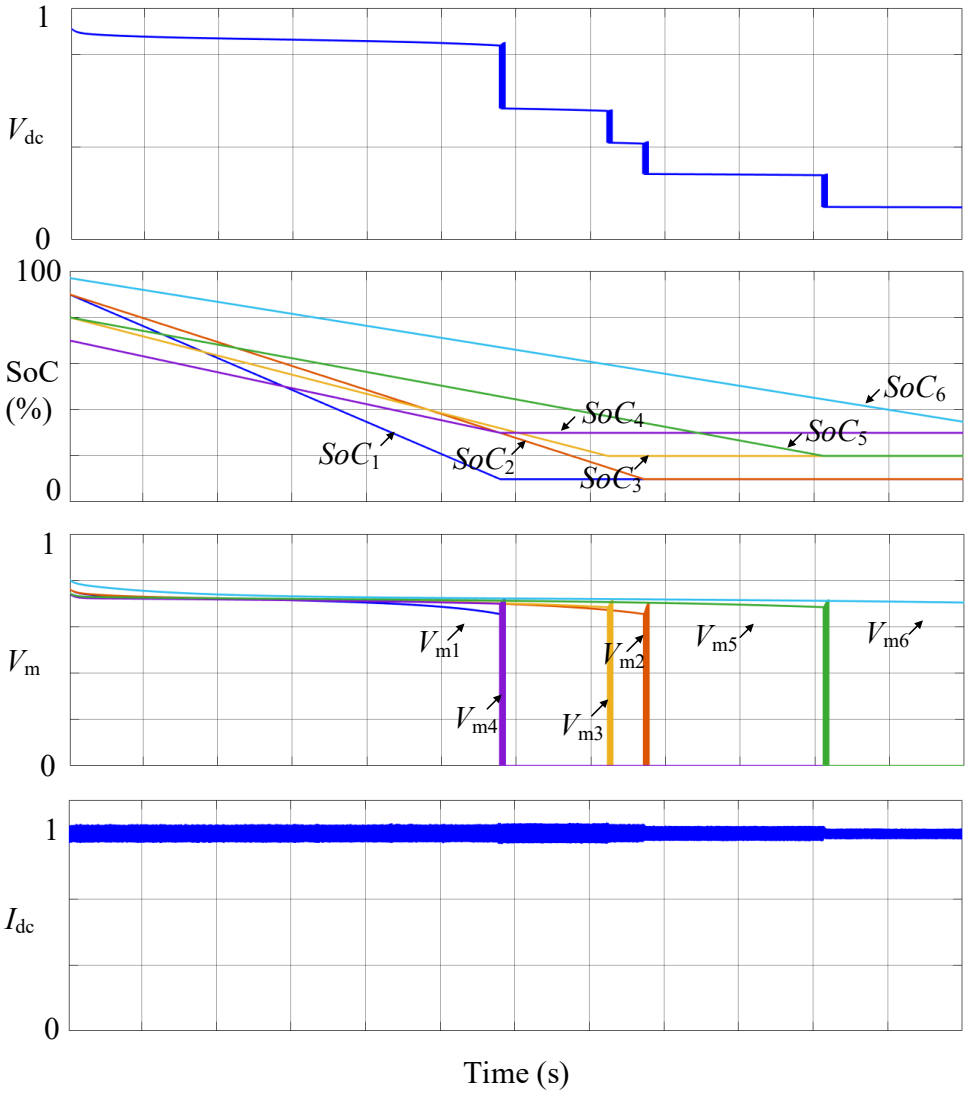

Fig. 4-5: Simulation results of the proposed system in discharging mode, illustrating dc-link voltage (V_{dc}), SoCs ($SoC_{1, ..., 6}$), module voltages ($V_{m1, ..., m6}$), and dc-link current (i_{dc}).

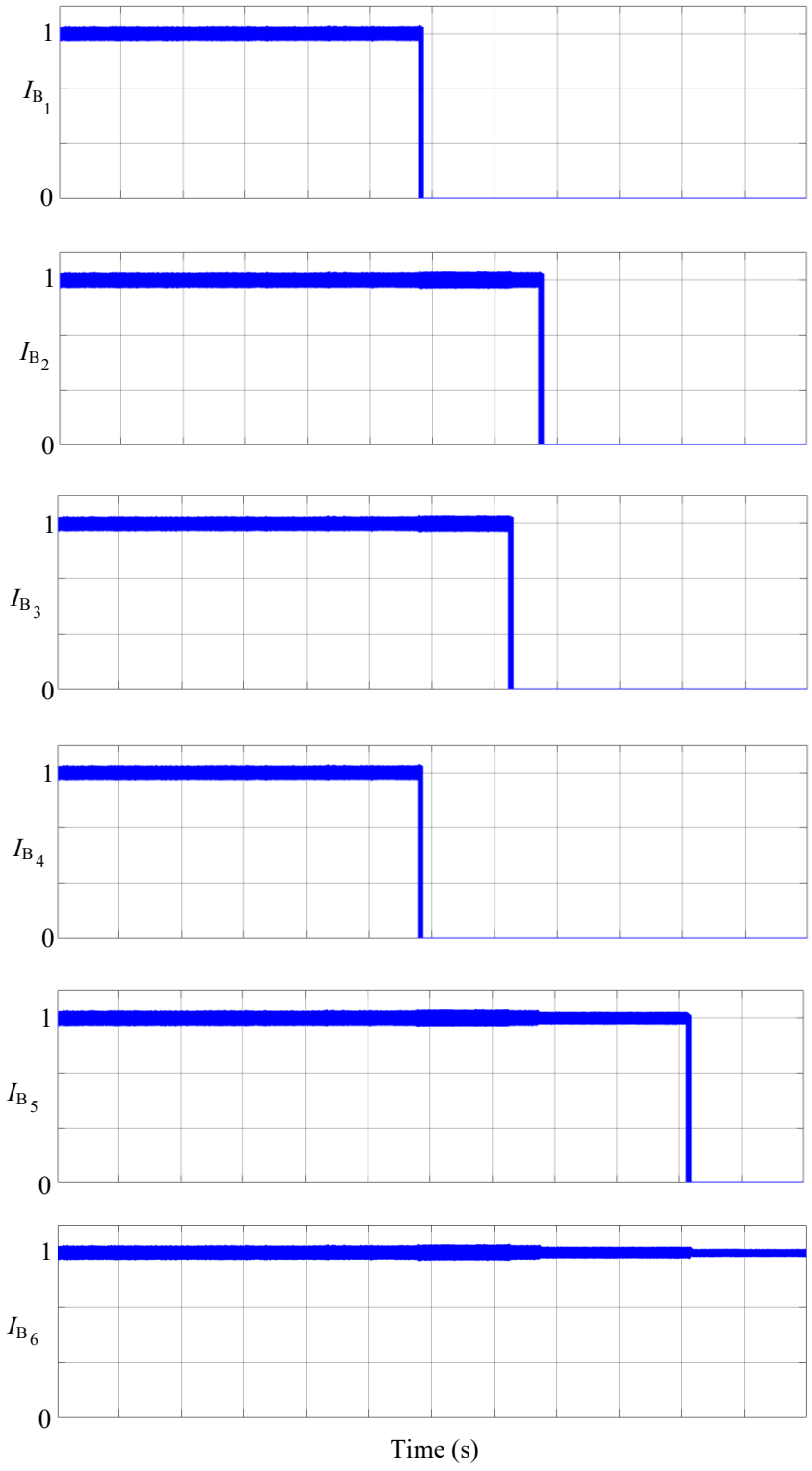

Fig. 4-6: Simulation results of the proposed system in discharging mode, illustrating battery currents ($I_{B1, \ldots, B6}$).

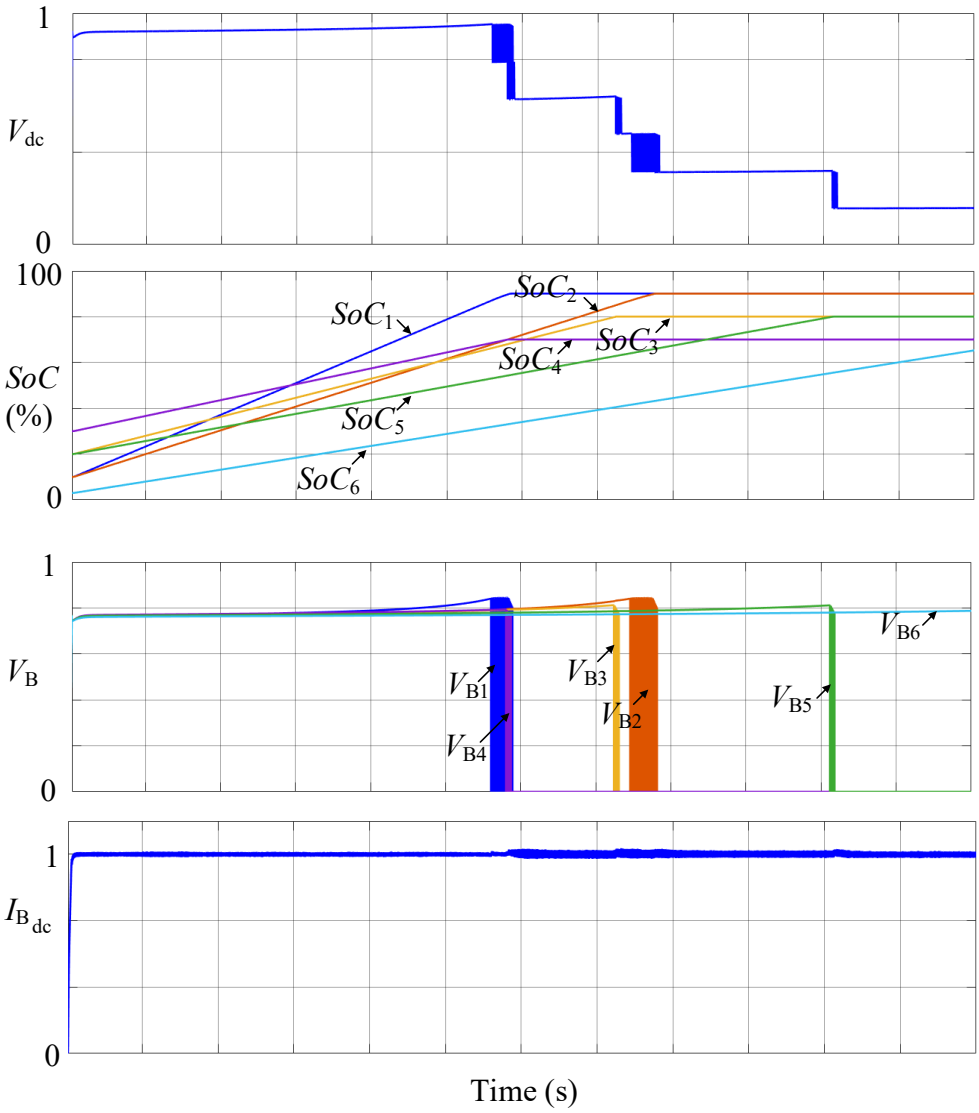

Fig. 4-7: Simulation results of the proposed system in charging mode, illustrating dc-link voltage (V_{dc}), SoCs ($SoC_{1, ..., 6}$), module voltages ($V_{m1, ..., m6}$), and dc-link current (i_{dc}).

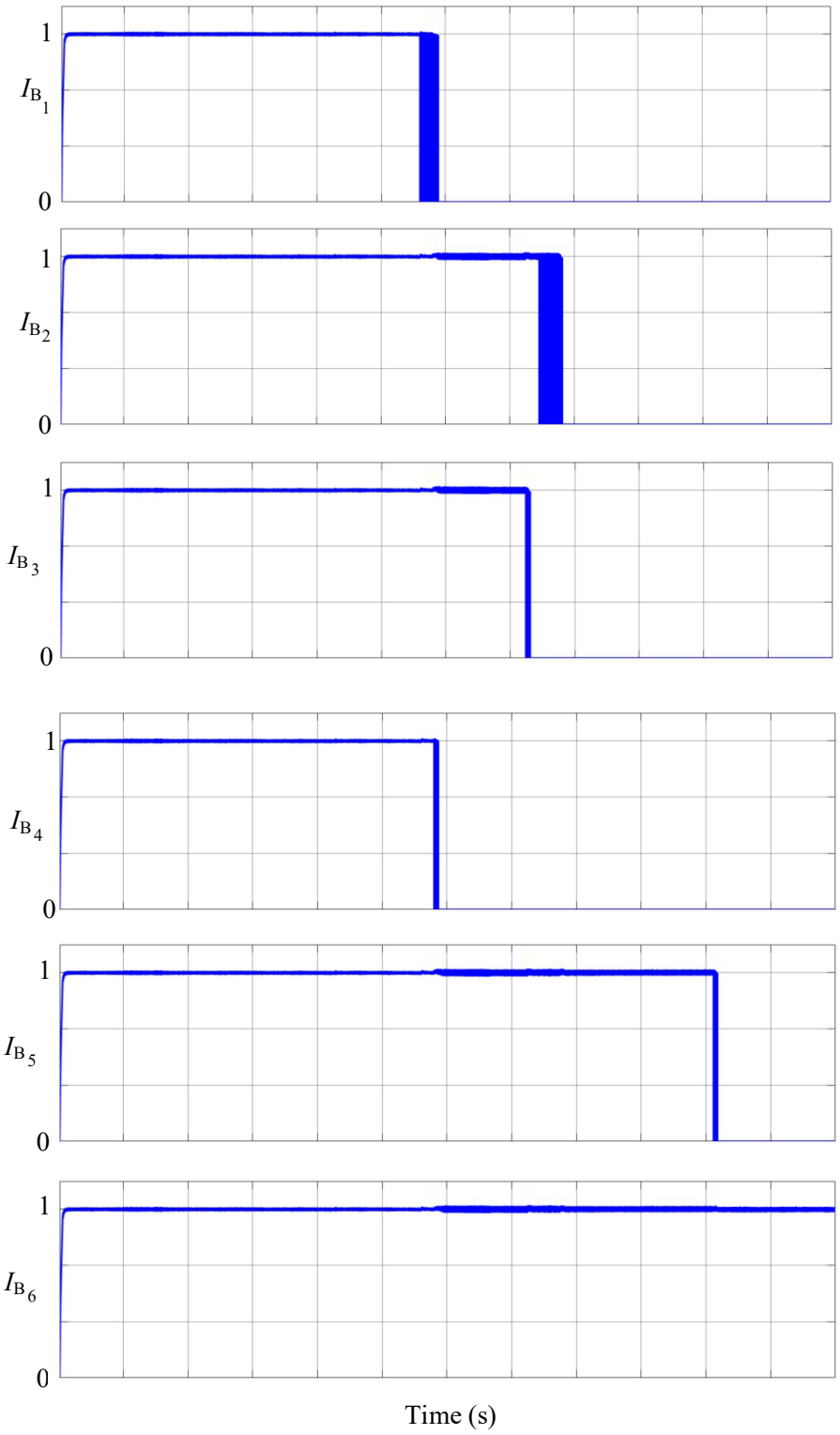

Fig. 4-8: Simulation results of the proposed system in charging mode, illustrating battery currents ($I_{B1, \ldots, B6}$).

4.5.2 Experimental Verification

Experimental validation was carried out on a laboratory-scale prototype of the proposed system. The complete hardware setup is shown in Fig. 4-9. The setup includes a grid simulator, CSC, and three modules, each connected to an independent bidirectional dc source (DC_1, DC_2, DC_3). The control strategy for the entire system was executed in real time using an OPAL-RT simulator.

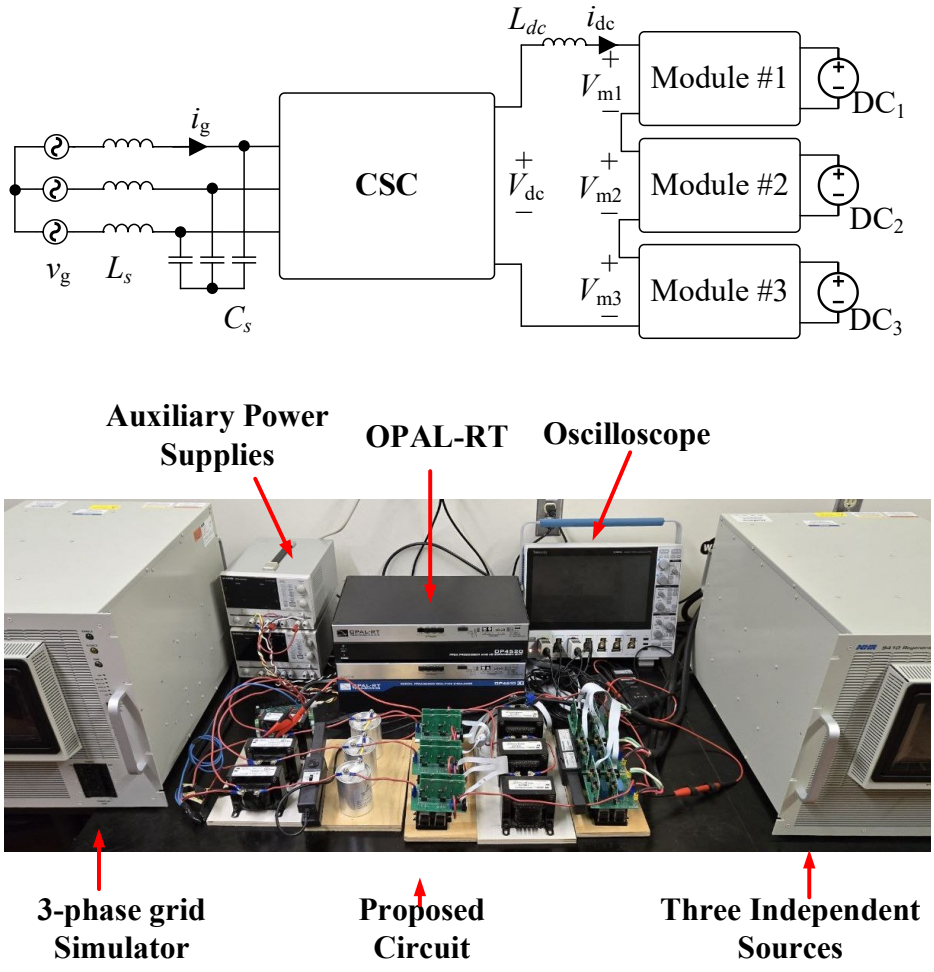

Fig. 4-9: Experimental setup.

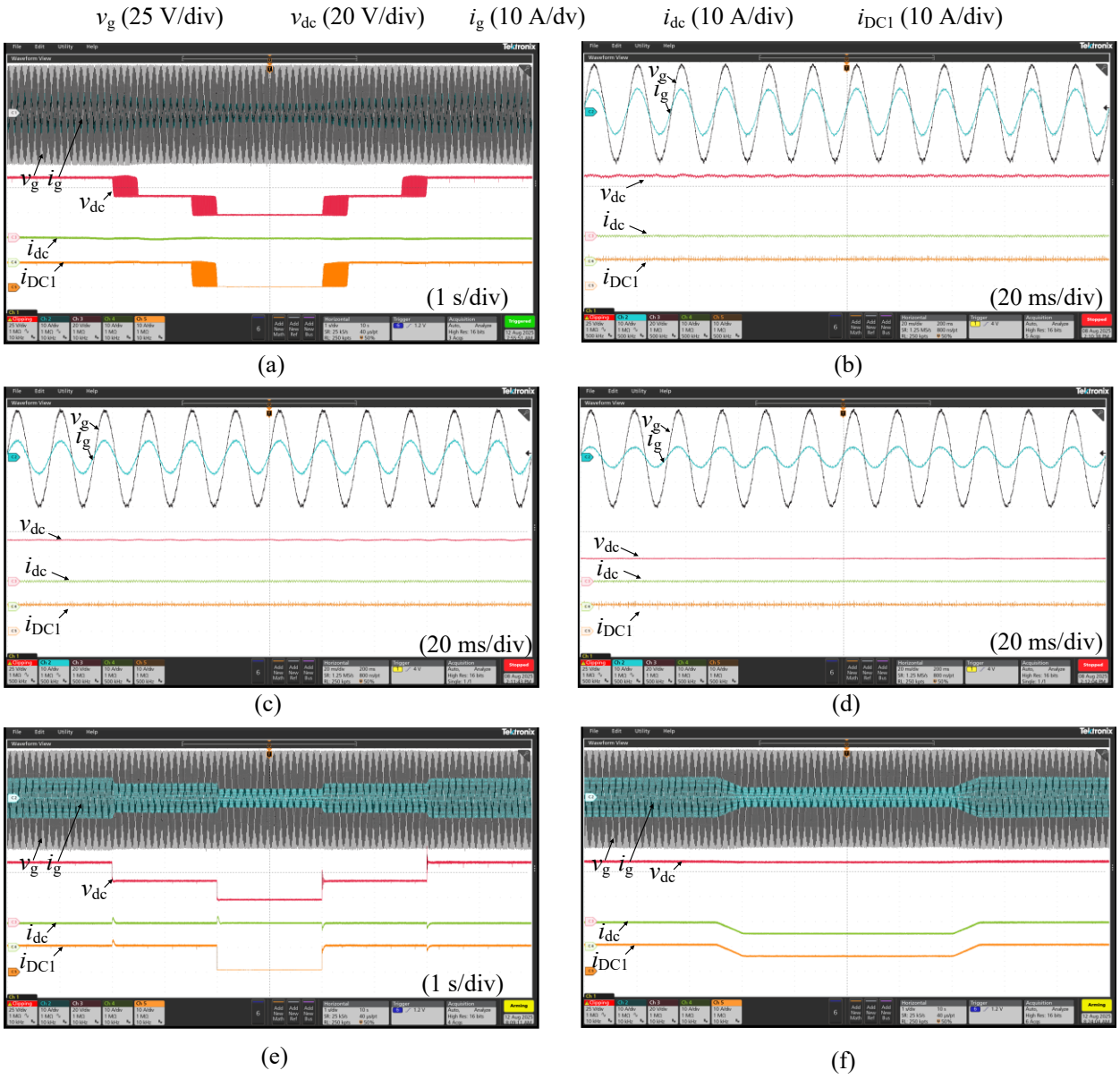

Fig. 4-10: Experimental waveforms for the system operating in discharge mode. (a) Dynamic operation. (b) Three active modules in CC mode. (c) Two active modules in CC mode. (d) One active module in CC mode. (e) Dynamic operation without a rate limiter. (f) Dynamic variation of the dc-link current.

Fig. 4-10 illustrates two discharging scenarios in which modules transition between active and bypass modes. The waveforms include the grid voltage (v_g) and current (i_g), the dc-link voltage (V_{dc}) and current (i_{dc}), and also the current of the first battery (i_{DC1}). In both cases, the output current is maintained at a constant 10 A. The operation of the system with a different number of active modules is presented in Fig. 4-10(b), Fig. 4-10(c), and Fig. 4-10(d). In Fig. 4-10(e), the impact of a rapid transition on the dc-link current is evident: a sudden change in module state introduces a transient in the current. When a rate limiter is applied, this effect is effectively mitigated, resulting in a smooth dc-link current profile without noticeable transients. In Fig. 4-10(f) The result of the system changing the i_{dc} current reference is shown as it is reduced to 0.5 pu. These results demonstrate the proposed system's ability to operate without an LFT and the need for complex balancing controls.

Similarly, Fig. 4-11 illustrates the operation of the system in charging mode, with a varying number of active modules. As charging progresses, the first and second module switches from CC mode to CV mode using pulsed current modulation, its current gradually reduces, until it is completely bypassed, with corresponding reductions in V_{dc} and i_g. While i_{dc} stays at 10 A. even in the case with only one active module, the CSR still regulates current effectively despite reduced V_{dc}, confirming stable operation.

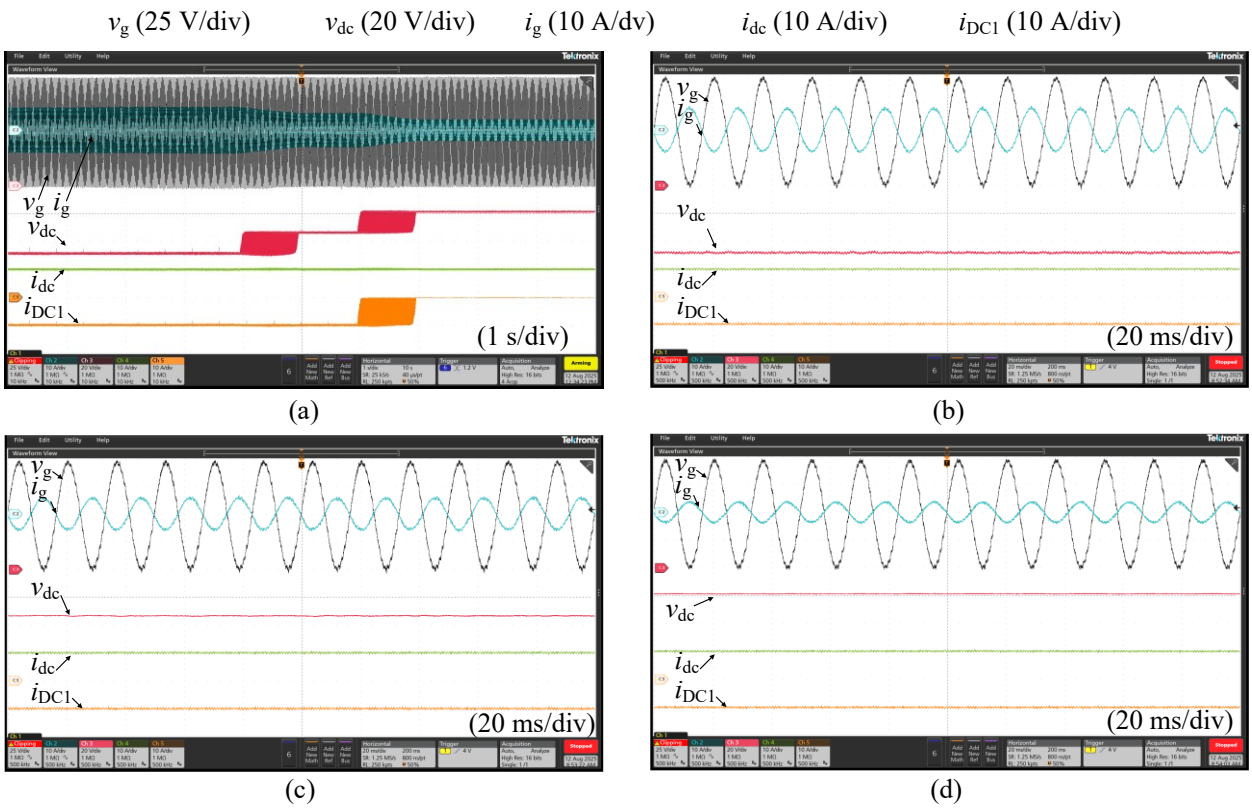

Fig. 4-11: Experimental waveforms for the system operating in charge mode. (a) Dynamic operation. (b) Three active modules in CC mode. (c) Two active modules in CC mode. (d) One active module in CC mode.

4.6 Chapter Summary

This chapter has presented the design, control, and validation of a CSC-based modular BESS topology capable of bidirectional operation with an MVAC grid. The proposed system integrates a series-connected battery configuration with a transformerless CSC interface, eliminating the need for bulky LFTs and complex SoC balancing hardware or controller. The architecture supports heterogeneous SLB modules by dynamically bypassing units, maintaining continuous operation and stable performance under various conditions. A hierarchical control strategy was developed to coordinate both grid-side and module-level operation, CC–CV regulation, and pulsed current operation. The variable dc-link voltage capability of the CSC allows the system to adapt to changes in the number of active modules without compromising dc-link current regulation. Simulation studies verified the system's performance under different scenarios, with the rate limiter effectively suppressing transients. Experimental validation on a scaled laboratory prototype further demonstrated the system's bidirectional operation, stable current regulation, and adaptability to different numbers of active modules.

Chapter 5: Conclusions and Future Work

The increasing deployment of utility-scale BESS for RESs integration and BESS charging applications has shown several technical challenges and practical limitations in existing architectures. Conventional low-voltage systems require step-up LFTs to interface with the MVAC grid, which are bulky, heavy, and costly. Modular high-voltage systems, while capable of operating without LFTs, introduce the need for complex balancing control strategies and additional hardware to manage variations in SoCs. These challenges lead to increased control complexity, reduced system flexibility, and potential limitations in scalability. These issues become more pronounced in systems directly interfacing with RESs, in modular battery charging infrastructures for BSSs, and in second-life BESS deployments, where variability in performance and reliability can undermine system stability and operational lifespan. Addressing these shortcomings formed the core motivation for the research presented in this thesis.

5.1 Contributions and Conclusions

This thesis presented the development, modeling, simulation, and experimental validation of three power conversion systems for large-scale MVAC-connected battery energy storage applications. The work addressed the limitations of both low-voltage architectures and LFT-less systems. The proposed system eliminates the need for LFTs and avoids the need for complex balancing control strategies or redundant hardware. and enabling stable operation under heterogeneous battery conditions. The research was divided into three main parts:

1. **A Current Source Inverter-Based BESS for Grid Integration of RESs (Chapter 2):**

The first part of the thesis developed and validated a CSI-based BESS architecture for direct MVAC connection in renewable energy applications. The design uses a string of modular low-voltage battery packs to achieve medium-voltage operation without an LFT. A detailed system model was built in MATLAB/Simulink, incorporating the grid interface, converter, and battery modules. Simulation studies demonstrated that the proposed topology maintains regulated output current and power under varying SoC conditions. Battery packs can be bypassed upon fault or depletion without disrupting operation. And the system was shown to handle severe SoC imbalances by bypassing depleted modules without disrupting grid current, and without requiring additional balancing hardware. Additional advantages include high scalability and inherent short-circuit protection. Both simulation and experimental results confirm that the CSI-based approach offers a viable alternative to LFT-based systems for direct RES–BESS grid integration, with reduced control complexity and improved fault tolerance.

2. **A Current Source Rectifier-Based Modular Battery Charging for BSSs (Chapter 3):**

The second part addressed the specific requirements of BSS charging infrastructure, which demands fast, scalable, and reliable battery charging. Conventional centralized and distributed charger systems share the same LFT dependency, while modular charging solutions require complex balancing or depend on offline balancing during low swapping demand. This work proposed a new modular CSR-based charging system directly interfaced to MVAC without an LFT. The architecture supports independent module operation and smooth disconnection of fully charged batteries through controlled CC/CV The proposed topology uses a two-part control system: a grid-side CSR controller for dc-link current and reactive power regulation, and a module-

level two-stage controller for CC–CV charging and pulsed-current modulation. This enables precise shaping of charging current for each battery and smooth handling of dynamic events such as module insertion, removal, and charging mode transitions. Simulation and experimental results confirmed operation under all tested scenarios, demonstrating its potential for a reliable, high-power BSS infrastructure that accommodates partial loading.

3. **A Current Source Converter-Based Modular BESS for Bidirectional Grid Integration (Chapter 4):**

A transformerless bidirectional CSC-based topology was developed for MVAC-connected BESS using heterogeneous second-life lithium-ion battery modules. The system supports both charging and discharging modes and allows bypassing weak modules based on SoC or health constraints without affecting the overall system operation. Simulation and experimental results showed that the system maintains stable grid operation without the need for LFT or complex balancing strategies under severe SoC range and capacity mismatches, and improves fault tolerance, confirming its suitability for SLB integration in medium-voltage grid-tied applications.

5.2 Future Work

Several opportunities exist to expand and enhance the concepts developed in this thesis. Potential research directions include extending system capabilities and exploring new deployment scenarios for the proposed MVAC-connected BESS architectures.

1. **Parallel String Operation and Coordination**

   Extend the proposed architecture to support multiple BESS strings operating in parallel at the MVDC level. This includes developing coordinated current-sharing algorithms to ensure uniform current distribution among strings despite differences in modules and synchronization of the dc-link variables.

2. **SOH Prediction and Degradation Modeling**

   Incorporate advanced state-of-health (SoH) estimation techniques to predict remaining useful life. SoH prediction will be essential in assessing operational boundaries of retired EV batteries, and optimization strategies can be designed to balance energy throughput, thermal conditions, and charge/discharge profiles across modules to minimize degradation rates. AI-based approaches can support SoH estimation and optimization, and an SOH-driven optimization framework would enhance the reliability of large-scale BESS deployments.

References

[1] X. Wu, C. Liu, R. Li, F. Wu, and X. Cai, “Four quadrant operation control for cascade H-bridge converter-based battery energy storage system,” *IEEE J. Emerg. Sel. Top. Ind. Electron.*, vol. 5, no. 3, pp. 1181–1191, 2024., doi: 10.1109/JESTIE.2024.3367633

[2] M. Ehsani, K. V. Singh, H. O. Bansal, and R. T. Mehrjardi, “State of the art and trends in electric and hybrid electric vehicles,” *Proc. IEEE*, vol. 109, no. 6, pp. 967–984, 2021., doi: 10.1109/JPROC.2021.3072788

[3] Y. Cao, J. Cui, S. Liu, X. Li, Q. Zhou, C. Hu, et al., “A holistic review on e-mobility service optimization: Challenges, recent progress, and future directions,” *IEEE Trans. Transp. Electrif.*, vol. 10, no. 2, pp. 3712–3741, 2023., doi: 10.1109/TTE.2023.3311410

[4] T. Boonraksa, P. Boonraksa, W. Pinthurat, and B. Marungsri, “Optimal Battery Charging Schedule for a Battery Swapping Station of an Electric Bus with a PV Integration Considering Energy Costs and Peak-to-Average Ratio,” *IEEE Access*, vol. 12, pp. 36280–36295, 2024., doi: 10.1109/ACCESS.2024.3374224

[5] X. Wang and J. Wang, “Economic assessment for battery swapping station based frequency regulation service,” *IEEE Trans. Ind. Appl.*, vol. 56, no. 5, pp. 5880–5889, 2020., doi: 10.1109/TIA.2020.2986186

[6] X. Wang, J. Wang, and J. Liu, “Vehicle to grid frequency regulation capacity optimal scheduling for battery swapping station using deep Q-network,” *IEEE Trans. Industr. Inform.*, vol. 17, no. 2, pp. 1342–1351, 2020., doi: 10.1109/TII.2020.2993858

[7] H. Wu, “A survey of battery swapping stations for electric vehicles: Operation modes and decision scenarios,” *IEEE Trans. Intell. Transp. Syst.*, vol. 23, no. 8, pp. 10163–10185, 2021., doi: 10.1109/TITS.2021.3125861

[8] X. Chen, K. Xing, F. Ni, Y. Wu, and Y. Xia, “An electric vehicle battery-swapping system: Concept, architectures, and implementations,” *IEEE Intell. Transp. Syst. Mag.*, vol. 14, no. 5, pp. 175–194, 2021., doi: 10.1109/MITS.2021.3119935

[9] X. Hu, X. Deng, F. Wang, Z. Deng, X. Lin, R. Teodorescu, et al., “A review of second-life lithium-ion batteries for stationary energy storage applications,” *Proc. IEEE*, vol. 110, no. 6, pp. 735–753, 2022., doi: 10.1109/JPROC.2022.3175614

[10] Y. Jiang, Y. Ke, F. Yang, J. Ji, and W. Peng, “State of health estimation for second-life lithium-ion batteries in energy storage system with partial charging-discharging workloads,” *IEEE Trans. Ind. Electron.*, vol. 71, no. 10, pp. 13178–13188, 2024., doi: 10.1109/TIE.2023.3344825

[11] Y. Ye, P. Huang, Z. Ke, and X. Wang, “Multiwinding Transformer Based Cell Balancing System With Cost-Effective Gate Drivers,” *IEEE Trans. Power Electron.*, vol. 40, no. 2, pp. 2685–2690, Feb. 2025., doi: 10.1109/TPEL.2024.3487189

[12] E. Nunes, G. Liang, E. Rodriguez, G. G. Farivar, and J. Pou, “Lifespan Maximization of Modular Battery Energy Storage Systems With State-of-Charge Imbalance Constraints,” *IEEE Trans. Ind. Electron.*, vol. 72, no. 6, pp. 6061–6071, Jun. 2025., doi: 10.1109/TIE.2024.3497299

[13] S. S. G. Acharige, M. E. Haque, M. T. Arif, N. Hosseinzadeh, K. N. Hasan, and A. M. T. Oo, “Review of electric vehicle charging technologies, standards, architectures, and converter configurations,” *IEEE Access*, vol. 11, pp. 41218–41255, 2023. doi: 10.1109/ACCESS.2023.3267164

[14] M. Liu, X. Cao, C. Cao, P. Wang, C. Wang, J. Pei, et al., “A review of power conversion systems and design schemes of high-capacity battery energy storage systems,” *IEEE Access*, vol. 10, pp. 52030–52042, 2022. doi: 10.1109/ACCESS.2022.3174193

[15] M. Rasheed, R. Hassan, M. Kamel, H. Wang, R. Zane, S. Tong, et al., “Active reconditioning of retired lithium-ion battery packs from electric vehicles for second-life applications,” *IEEE J. Emerg. Sel. Top. Power Electron.*, vol. 12, no. 1, pp. 388–404, 2023. doi: 10.1109/JESTPE.2023.3325251

[16] X. Li, L. Lyu, G. Geng, Q. Jiang, Y. Zhao, F. Ma, et al., “Power allocation strategy for battery energy storage system based on cluster switching,” *IEEE Trans. Ind. Electron.*, vol. 69, no. 4, pp. 3700–3710, 2021. doi: 10.1109/TIE.2021.3076731

[17] G. Wang, G. Konstantinou, C. D. Townsend, J. Pou, S. Vazquez, G. D. Demetriades, et al., “A review of power electronics for grid connection of utility-scale battery energy storage systems,” *IEEE Trans. Sustain. Energy*, vol. 7, no. 4, pp. 1778–1790, 2016. doi: 10.1109/TSTE.2016.2586941

[18] G. G. Farivar, W. Manalastas, H. D. Tafti, S. Ceballos, A. Sanchez-Ruiz, E. C. Lovell, et al., “Grid-connected energy storage systems: State-of-the-art and emerging technologies,” *Proc. IEEE*, vol. 111, no. 4, pp. 397–420, 2022. doi: 10.1109/JPROC.2022.3183289

[19] H. Tu, H. Feng, S. Srdic, and S. Lukic, “Extreme fast charging of electric vehicles: A technology overview,” *IEEE Trans. Transp. Electrif.*, vol. 5, no. 4, pp. 861–878, 2019. doi: 10.1109/TTE.2019.2958709

[20] “PCS100 ESS - Power Converters and Controllers | Power Converters and Controllers | ABB.” Accessed: Aug. 06, 2025. [Online]. Available: https://new.abb.com/power-converters-inverters/power-converters-and-inverters/pcs100-ess

[21] "Energy Storage System Products List | HUAWEI Smart PV Global." Accessed: Aug. 13, 2025. [Online]. Available: https://solar.huawei.com/en/products/energy-storage-system/

[22] L. Maharjan, T. Yamagishi, and H. Akagi, "Active-power control of individual converter cells for a battery energy storage system based on a multilevel cascade PWM converter," *IEEE Trans. Power Electron.*, vol. 27, no. 3, pp. 1099–1107, 2010. doi: 10.1109/TPEL.2010.2059045

[23] G. F. Gontijo, T. Kerekes, D. Sera, M. Ricco, L. Mathe, and R. Teodorescu, "Medium-voltage converter solution with modular multilevel structure and decentralized energy storage integration for high-power wind turbines," *IEEE Trans. Power Electron.*, vol. 36, no. 11, pp. 12954–12967, 2021. doi: 10.1109/TPEL.2021.3077501

[24] P. Poblete, R. H. Cuzmar, R. P. Aguilera, J. Pereda, A. M. Alcaide, D. Lu, et al., "Dual-Stage MPC for SoC Balancing in Second-Life Battery Energy Storage Systems Based on Delta-Connected Cascaded H-Bridge Converters," *IEEE Trans. Power Electron.*, vol. 40, no. 1, pp. 500–515, Jan. 2025., doi: 10.1109/TPEL.2024.3461749

[25] Q. Xiao, H. Yu, Y. Jin, H. Jia, Y. Mu, H. Liu, et al., "A Novel Fault-Tolerant Operation Approach for Cascaded H-Bridge Converter-Based Battery Energy Storage Systems to Avoid Overcharge," *IEEE Trans. Ind. Electron.*, vol. 72, no. 6, pp. 5497–5506, Jun. 2025., doi: 10.1109/TIE.2024.3485716

[26] M. Vasiladiotis and A. Rufer, "Analysis and control of modular multilevel converters with integrated battery energy storage," *IEEE Trans. Power Electron.*, vol. 30, no. 1, pp. 163–175, 2014. doi: 10.1109/TPEL.2014.2303297

[27] Q. Zhang and K. Sun, “A flexible power control for PV-battery hybrid system using cascaded H-bridge converters,” *IEEE J. Emerg. Sel. Top. Power Electron.*, vol. 7, no. 4, pp. 2184–2195, 2018. doi: 10.1109/JESTPE.2018.2887002

[28] S. Nayak, A. Das, R. E. Torres-Olguin, S. D’Arco, and G. Guidi, “Battery energy support to cascaded H-bridge converter-fed large-scale PV system during unbalanced power generation,” *IEEE Trans. Ind. Appl.*, vol. 58, no. 6, pp. 7479–7489, 2022. doi: 10.1109/TIA.2022.3200648

[29] D. Iannuzzi, M. Coppola, P. Guerriero, A. Dannier, and A. Del Pizzo, “Power Scheduling Method for Grid Integration of a PV-BESS CHB Inverter with SOC Balancing Capability,” *IEEE Access*, vol. 10,112273–112285, 2022. doi: 10.1109/ACCESS.2022.3215270

[30] Z. Ma, F. Gao, X. Gu, N. Li, Q. Wu, X. Wang, et al., “Multilayer SOH equalization scheme for MMC battery energy storage system,” *IEEE Trans. Power Electron.*, vol. 35, no. 12, pp. 13514–13527, 2020. doi: 10.1109/TPEL.2020.2991879

[31] G. Liang, G. G. Farivar, S. Ceballos, H. D. Tafti, J. Pou, C. D. Townsend, et al., “Unbalanced active power distribution of cascaded multilevel converter-based battery energy storage systems,” *IEEE Trans. Ind. Electron.*, vol. 69, no. 12, pp. 13022–13032, 2021. doi: 10.1109/TIE.2021.3137442

[32] H. Akagi, “Classification, terminology, and application of the modular multilevel cascade converter (MMCC),” *IEEE Trans. Power Electron.*, vol. 26, no. 11, pp. 3119–3130, 2011. doi: 10.1109/TPEL.2011.2143431

[33] N. Li, F. Gao, T. Hao, Z. Ma, and C. Zhang, “SOH balancing control method for the MMC battery energy storage system,” *IEEE Trans. Ind. Electron.*, vol. 65, no. 8, pp. 6581–6591, 2017. doi: 10.1109/TIE.2017.2733462

[34] C. Liu, N. Gao, X. Cai, and R. Li, "Differentiation power control of modules in second-life battery energy storage system based on cascaded H-bridge converter," *IEEE Trans. Power Electron.*, vol. 35, no. 6, pp. 6609–6624, 2019. doi: 10.1109/TPEL.2019.2954577

[35] B. Xu, H. Tu, Y. Du, H. Yu, H. Liang, and S. Lukic, "A distributed control architecture for cascaded H-bridge converter with integrated battery energy storage," *IEEE Trans. Ind. Appl.*, vol. 57, no. 1, pp. 845–856, 2020. doi: 10.1109/TIA.2020.3039430

[36] I. Marzo, A. Sanchez-Ruiz, J. A. Barrena, G. Abad, and I. Muguruza, "Power balancing in cascaded H-bridge and modular multilevel converters under unbalanced operation: A review," *IEEE Access*, vol. 9,110525–110543, 2021. doi: 10.1109/ACCESS.2021.3103337

[37] A. Lashab, D. Sera, F. Hahn, L. J. Camurca, M. Liserre, and J. M. Guerrero, "A reduced power switches count multilevel converter-based photovoltaic system with integrated energy storage," *IEEE Trans. Ind. Electron.*, vol. 68, no. 9, pp. 8231–8240, 2020. doi: 10.1109/TIE.2020.3009594

[38] H. Xue and J. He, "Flexible power control for extending operating range of PV–Battery hybrid cascaded H-bridge converters under unbalanced power conditions," *IEEE Trans. Ind. Electron.*, vol. 70, no. 8, pp. 8118–8128, 2022. doi: 10.1109/TIE.2022.3229317

[39] G. Liang, E. Rodriguez, G. G. Farivar, E. Nunes, G. Konstantinou, C. D. Townsend, et al., "Model Predictive Control for Intersubmodule State-of-Charge Balancing in Cascaded H-Bridge Converter-Based Battery Energy Storage Systems," *IEEE Trans. Ind. Electron.*, vol. 71, no. 6, pp. 5777–5786, Jun. 2024., doi: 10.1109/TIE.2023.3290249

[40] Z. Li, R. Lizana, S. M. Lukic, A. V. Peterchev, and S. M. Goetz, "Current injection methods for ripple-current suppression in delta-configured split-battery energy storage," *IEEE Trans. Power Electron.*, vol. 34, no. 8, pp. 7411–7421, 2018. doi: 10.1109/TPEL.2018.2879613

[41] Z. Ma, F. Gao, C. Zhang, W. Li, and D. Niu, "Variable DC-link voltage regulation of single-phase MMC battery energy-storage system for reducing additional charge throughput," *IEEE Trans. Power Electron.*, vol. 36, no. 12, pp. 14267–14281, 2021. doi: 10.1109/TPEL.2021.3084605

[42] H. Xue, J. He, Y. Ren, and P. Guo, "Seamless fault-tolerant control for cascaded H-bridge converters based battery energy storage system," *IEEE Trans. Ind. Electron.*, vol. 70, no. 4, pp. 3803–3813, 2022. doi: 10.1109/TIE.2022.3177789

[43] W. Jiang, C. Zhu, S. Xue, K. Ren, and C. Yang, "DC-side-fault-tolerant control of a battery-supercapacitor hybrid energy storage system based on cascaded multilevel converter and auxiliary power loop," *IEEE Trans. Ind. Electron.*, vol. 67, no. 9, pp. 7451–7460, 2019. doi: 10.1109/TIE.2019.2942573

[44] N. Mukherjee and D. Strickland, "Analysis and comparative study of different converter modes in modular second-life hybrid battery energy storage systems," *IEEE J. Emerg. Sel. Top. Power Electron.*, vol. 4, no. 2, pp. 547–563, 2015. doi: 10.1109/JESTPE.2015.2460334

[45] L. Maharjan, S. Inoue, H. Akagi, and J. Asakura, "State-of-charge (SOC)-balancing control of a battery energy storage system based on a cascade PWM converter," *IEEE Trans. Power Electron.*, vol. 24, no. 6, pp. 1628–1636, 2009. doi: 10.1109/TPEL.2009.2014868

[46] E. Chatzinikolaou and D. J. Rogers, "Cell SoC balancing using a cascaded full-bridge multilevel converter in battery energy storage systems," *IEEE Trans. Ind. Electron.*, vol. 63, no. 9, pp. 5394–5402, 2016. doi: 10.1109/TIE.2016.2565463

[47] A. Gohari, H. Althuwaini, and M. B. Shadmand, "Optimal utilization of battery sources in cascaded h-bridge inverter by coordinated sequence selection," *IEEE Trans. Ind. Electron.*, vol. 71, no. 9, pp. 10841–10853, 2023. doi: 10.1109/TIE.2023.3335462

[48] M. Barresi, D. De Simone, and L. Piegari, “Direct State-of-Charge Balancing Control for Modular Multilevel Converter Integrating Batteries,” *IEEE J. Emerg. Sel. Top. Power Electron.*, vol. 13, no. 1, pp. 733–746, Feb. 2025., doi: 10.1109/JESTPE.2024.3510876

[49] G. Liang, H. D. Tafti, G. G. Farivar, J. Pou, C. D. Townsend, G. Konstantinou, et al., “Analytical derivation of intersubmodule active power disparity limits in modular multilevel converter-based battery energy storage systems*,” IEEE Trans. Power Electron.*, vol. 36, no. 3, pp. 2864–2874, 2020. doi: 10.1109/TPEL.2020.3014739

[50] G. Liang, E. Rodriguez, G. G. Farivar, S. Ceballos, C. D. Townsend, N. B. Y. Gorla, et al., “A constrained intersubmodule state-of-charge balancing method for battery energy storage systems based on the cascaded H-bridge converter,” *IEEE Trans. Power Electron*., vol. 37, no. 10, pp. 12669–12678, 2022. doi: 10.1109/TPEL.2022.3170062

[51] Y. Ma, J. Xiao, H. Lin, and Z. Wang, “A novel battery integration method of modular multilevel converter with battery energy storage system for capacitor voltage ripple reduction,” *IEEE Trans. Ind. Electron.*, vol. 68, no. 12, pp. 12250–12261, 2020. doi: 10.1109/TIE.2020.3044780

[52] Y. Huang, F. Liu, Y. Zhuang, X. Diao, Y. Lei, and H. Zhu, “Bidirectional Three-Port Converter for Modular Multilevel Converter-Based Retired Battery Energy Storage Systems,” *IEEE Trans. Power Electron.*, vol. 39, no. 9, pp. 11148–11163, 2024. doi: 10.1109/TPEL.2024.3388844

[53] E. Chatzinikolaou and D. J. Rogers, “A comparison of grid-connected battery energy storage system designs,” *IEEE Trans. Power Electron.*, vol. 32, no. 9, pp. 6913–6923, 2016. doi: 10.1109/TPEL.2016.2629020

[54] M. Liu, W. Li, C. Wang, M. P. Polis, and J. Li, “Reliability evaluation of large-scale battery energy storage systems,” *IEEE Trans. Smart Grid,* vol. 8, no. 6, pp. 2733–2743, 2016. doi: 10.1109/TSG.2016.2536688

[55] A. Manenti, A. Abba, A. Merati, S. M. Savaresi, and A. Geraci, “A new BMS architecture based on cell redundancy,” *IEEE Trans. Ind. Electron.*, vol. 58, no. 9, pp. 4314–4322, 2010. doi: 10.1109/TIE.2010.2095398

[56] B. Yildirim, M. A. Elgendy, A. N. Smith, and V. Pickert, “Efficiency optimized power-sharing algorithm for modular battery energy storage systems*,” IEEE Trans. Ind. Electron.*, vol. 70, no. 11, pp. 11299–11309, 2022. doi: 10.1109/TIE.2022.3229311

[57] Z. Ma, X. Yi, W. Li, F. Gao, and F. Yu, “Sorting selection balancing control for the modular multilevel DC/DC converter in battery swapping stations,” in *Proc. IEEE Energy Convers. Congr. Expo. (ECCE)*, Vancouver, BC, Canada, Oct. 2021, pp. 1730–1734, doi: 10.1109/ECCE47101.2021.9595936.

[58] Z. Ma, F. Gao, W. Li, M. Jia, D. Wasylowski, Q. Lv, et al., “Two-Mode Balancing Control Scheme for Modular DC/DC Converter Interfaced Battery Swapping Stations,” *IEEE Trans. Transp. Electrif.*, vol. 11, no. 1, pp. 1640–1651, Feb. 2025., doi: 10.1109/TTE.2024.3408897

[59] S. Nayak and A. Das, “A Power Balancing Strategy in a PV-Based Modular Multilevel Converter During Mismatched Power Generation,” *IEEE Trans. Ind. Electron.*, vol. 71, no. 7, pp. 7117–7125, Jul. 2024., doi: 10.1109/TIE.2023.3303654

[60] J. Li, J. Chen, C. Gong, and Q. He, “Improved Square Wave Injection Strategy for the Voltage Balance Control of Cascaded H-Bridge Rectifier*,” IEEE Trans. Transp. Electrif.*, vol. 9, no. 3, pp. 3711–3722, 2023. doi: 10.1109/TTE.2023.3244543

[61] R. He, K. Tian, and Z. Ling, “Offline Equalization Control of Modular Multilevel Converter-Based Battery Energy Storage System,” *IEEE Trans. Ind. Electron.*, vol. 71, no. 8, pp. 9003-9012, Aug. 2024, doi: 10.1109/TIE.2023.3331145.

[62] B. Wu and M. Narimani, High-power converters and AC drives. John Wiley & Sons, 2017. doi: 10.1002/9781119156079

[63] L. Xing, Q. Wei, and Y. Li, “A Practical Current Source Inverter-Based High-Power Medium-Voltage PV System,” *IEEE Trans. Power Electron.*, vol. 38, no. 2, pp. 2617–2625, 2022. doi: 10.1109/TPEL.2022.3211409